

# Integrated earthquake locations and magnitudes plus focal mechanisms for the North Sea & construction of a velocity model

Deliverable 2.1



<b>Organisation(s)</b>	Delft University of Technology, <i>NORSAR</i> , <i>GEUS</i> , <i>University of Oxford</i> , <i>BGS</i> , <i>Equinor</i> , <i>Shell</i> , and <i>BP</i>
<b>Author(s)</b>	Cornelis Weemstra, Tom Kettlety, Daniela Kühn, Evgeniia Martuganova, Johannes Schweitzer, Brian Baptie, Trine Dahl-Jensen
<b>Reviewers</b>	Auke Barnhoorn (TU Delft) & Tine Larsen (GEUS)
<b>Type of deliverable</b>	Database & Report
<b>WP</b>	2
<b>Issue date</b>	October 19, 2022
<b>Document version</b>	1

**Keywords:** North Sea seismicity, North Sea Seismic bulletin, P-wave velocity model, North Sea focal mechanism database

## Summary:

This report, together with an accompanying North Sea bulletin, constitutes Deliverable 2.1 of SHARP Storage. It is the result of the activities within task 2.1 of work package 2 of this project. Seismic event data was requested from all relevant data providers bordering the North Sea. The combined list of events has subsequently been cleaned, and duplicate events have been removed. An initial statistical analysis of the catalogue has been provided, including a magnitude-frequency distribution and associated Gutenberg-Richter b-value. In addition, a focal mechanism catalogue has been created, and an overview and analysis of the available velocity models relevant for the North Sea area are presented. In the next two years, the bulletin and the focal mechanism catalogue will be updated and augmented with more (lower magnitude) event data, ultimately resulting in deliverable 2.4 of SHARP Storage.

# 1. Introduction

The North Sea hosts a large number of sites for which Carbon Capture and Sequestration (CCS) is proposed. Many of the proposed reservoirs, which are mostly in saline aquifers (e.g., Greater Bunter Sandstone, Lisa), are in areas in which little to no borehole stress data is available. An accurate and dense observation of the present-day stress field, however, is important to understand and anticipate the response of the reservoir and caprock to large-scale fluid injection over prolonged periods, and hence to design an appropriate injection program. Seismic monitoring over several years revealed that (small) earthquakes occur widely in the North Sea. Especially focal mechanisms of earthquakes are very good indicators of present-day crustal dynamics. These earthquakes have the potential to add valuable insight into the present-day stress field in areas outside the main hydrocarbon provinces.

In practice, inverting seismological data for focal mechanisms was a challenge in the North Sea due to sparse and uneven station distribution. Detailed moment tensor solutions were only obtained for few selected events (usually for magnitudes  $> 3.5$ ) in the North Sea (e.g., Cesca et al., 2011; Jerkins et al., 2020). The situation has improved in recent years with the addition of several permanent (hydrocarbon)-reservoir monitoring (PRM) systems that are increasingly utilized for regional earthquake monitoring (Zarifi et al., 2021). Nevertheless, seismological data are scattered over various national agencies bordering the North Sea shores, and typically comprise non-public operator-owned data offshore. The different uses of the various networks imply significant differences in instrumentation ranging from vaulted broadband stations on land to short-period geophone or fiber optic cables offshore.

The ambition of SHARP is to combine the available data for a holistic and step-wise improvement of North Sea seismicity bulletins. This report is therefore accompanied by an integrated earthquake bulletin for the North Sea area. Together, this report and the bulletin constitute Deliverable 2.1 (D2.1) of SHARP Storage and present the results of the activities within task 2.1 of work package 2 (WP2). Note that in section 2, we provide a more detailed description of the embedding of D2.1 within the SHARP Storage project. Deliverable 2.1 reads: *'Integrated earthquake locations and magnitudes plus focal mechanisms for the North Sea & construction of a velocity model'*. Therefore, in addition to a description of the North Sea bulletin, this report also includes a first step towards an integrated velocity model for the North Sea area (Section 5).

Finally, and importantly, we define the terms 'event', 'catalogue' and 'bulletin'. With an 'event', we refer to a specific unique earthquake or explosion that resulted in distinct arrivals at a set of stations. 'Catalogue' refers to a list of unique events, each with a single origin time, location, and magnitude. In practice, each line of a catalogue therefore corresponds to a single unique event. 'Bulletin', instead, refers to a more complete description of event data. In a bulletin, each event can have several measured origin times and locations, and phase readings are included. Generally speaking, catalogues are produced from the bulletins, with each event (i.e., each line) in the catalogue corresponding to the 'prime' origin in the bulletin (each event in a bulletin has a single origin that is designated the prime origin).

## 1.1 Outlook

Although deliverable 2.1 (D2.1) is a necessary first step towards an integrated North Sea bulletin, the final objective will be deliverable 2.4 (see also Section 2). By combining seismic data from various onshore and offshore networks, we will be able to not only improve the detection threshold of local and regional seismicity in the vicinity of the planned CCS sites, but also to significantly improve location and focal mechanism uncertainty. Existing seismicity catalogues and bulletins for the North Sea are far from complete and are in general only including larger magnitude events ( $M_L > 3$ ). Small earthquakes are typically recorded on fewer seismographs than larger ones, and it is therefore crucial to include all available data. As earthquakes smaller than  $M_L 3.0$  are underreported to international agencies, data integration among neighbouring countries is an important part of the process (Figure 1.1). For D2.4, we will work on an updated and expanded bulletin towards lower magnitude events. By applying advanced event location methodologies and a probabilistic approach for focal mechanism analysis, we expect to significantly improve the bulletin described below and to include smaller events with lower signal-to-noise ratios. Since a good velocity model is a prerequisite for the bulletin improvement, we will also establish a velocity model, compare it to available ones and evaluate the necessary resolution. As part of updating the bulletin, different magnitude scales will be compared, and scaling relations may be estimated. Software for the probabilistic characterisation of focal mechanisms will be developed within this task and will be made publicly available.

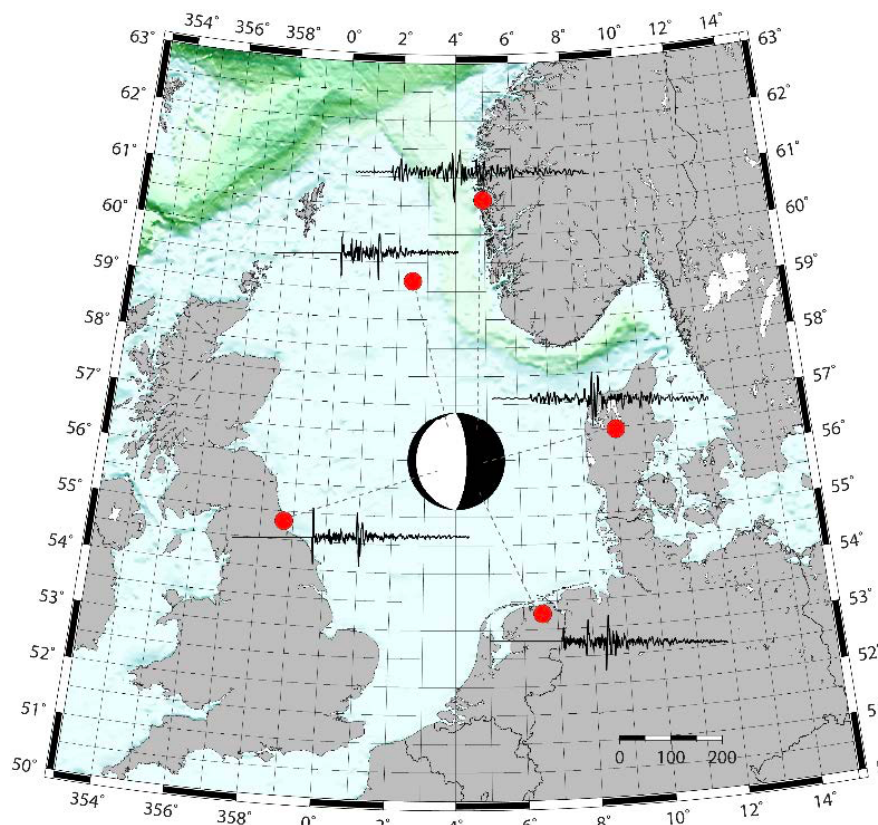


*Figure 1.1: Visualisation of the envisaged integrated moment tensor inversion by combining recordings of onshore, offshore, and temporary seismic stations from various data centres and industry partners.*

## 2. Context within SHARP Storage

The primary objective of the SHARP Storage project is to ‘increase the accuracy for subsurface CO<sub>2</sub> storage containment risk management by improvement and integration of models for subsurface stress, rock mechanical failure and seismicity in order to mature the technology for quantification of subsurface deformation and cost-efficient CO<sub>2</sub> subsurface risk management’. By meeting this objective, the project will accelerate the maturation of storage sites in the North Sea and India. Examples of sites that are expected to benefit are the Northern Lights CO<sub>2</sub> storage project in the Horda area (Norway), the Greater Bunter Sandstone area (United Kingdom), and the Lisa structure (Denmark). Involvement of the responsible CO<sub>2</sub> storage operators in the consortium will ensure that the SHARP project will have a high impact on CCS development of those storage sites.

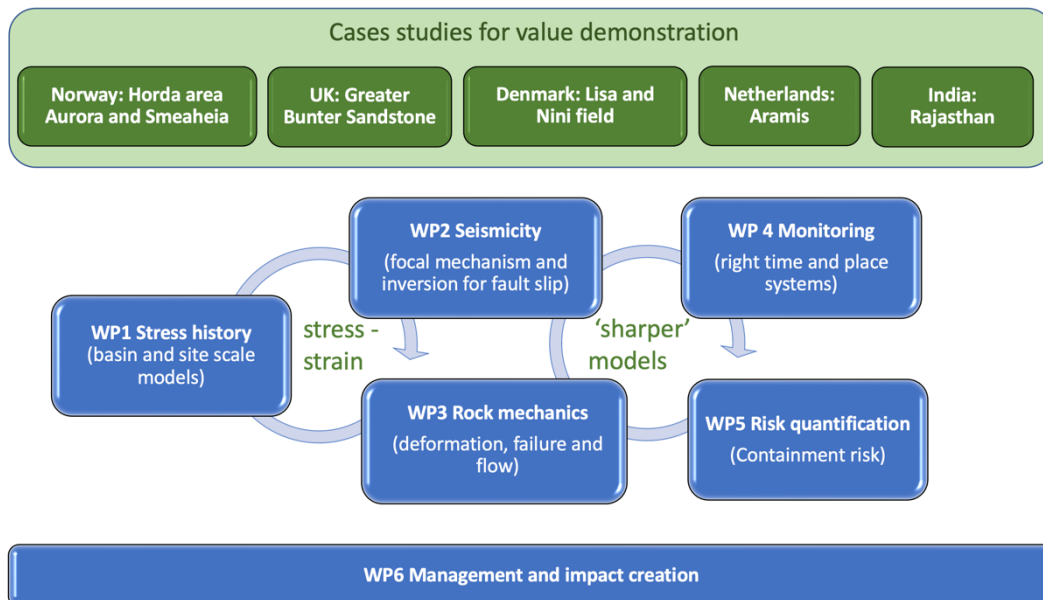


Figure 2.1: Relation between the various WPs within SHARP Storage. Deliverable 2.1, which we report on here, is one of the four deliverables within WP2. Institutes and companies involved in Task 2.1 (and hence D2.1) are Delft University of Technology, NORSTAR, GEUS, University of Oxford, BGS, Equinor, Shell, and BP.

To meet SHARP Storage’s primary objective, several secondary objectives, milestones, and deliverables have been formulated. Furthermore, the project is divided into six work packages (WPs; see Figure 2.1). Each WP has a defined leader, a specific work description, and is associated with a subset of milestones and deliverables. Together, the constructed integrated earthquake bulletin and this document make up D2.1. This deliverable is one of the four deliverables within WP2. This work package aims to ‘improve knowledge of the present-day stress field in the North Sea from integrated earthquake bulletins and provide a comprehensive database of earthquake focal mechanisms’. In addition to deliverable 2.1, three other deliverables (D2.2, D2.3, and D2.4) will help to achieve this aim. These other deliverables focus on stress drop estimation (D2.2) as well as anisotropy (D2.3) and provide an updated bulletin and focal mechanism database (D2.4). The latter deliverable builds on D2.1 by augmenting it with the centroid-moment tensor inversion results obtained within task 2.1 (see



SHARP Storage – Project no 327342



Section 1.1). Successful preparation of these deliverables will ultimately provide mission-critical insights on caprock integrity around the case study sites and provide valuable insights on actively slipping faults.

## 3. Rectangular North Sea bulletin

An initial step to a comprehensive North Sea bulletin involves gathering all available events in the North Sea region. We refer to this bulletin as the 'rectangular bulletin', since we collected all events within a specified rectangular area containing the North Sea. These events are requested from all relevant data providers (data centres, universities, regional authorities, etc.). These data providers are described in Section 3.1. In Section 3.2, we introduce the format in which the bulletin is stored and published, for which we adopted the widely used and recognised ISF format. This format does not only apply to the rectangular bulletin: the same format is used for the publication of this stage's bulletin (i.e., D2.1). In Section 3.3, we present the details and parameters (e.g., latitude and longitude boundaries) associated with the rectangular bulletin.

### 3.1 Contributing data providers

Below, we describe one by one the different data centres and providers from which event data was retrieved. These are international, national, and regional in scope. Some of these data centres are associated with countries that have little overlap with the North Sea area, whereas others have significantly more. This implies that the contribution of individual data providers towards the rectangular bulletin varies widely.

#### 3.1.1 International Seismological Centre

Under the umbrella of the International Association of Seismology and Physics of the Earth's Interior (IASPEI), the International Seismological Centre (ISC) always played an important role in setting up international standards such as the International Seismic bulletin Format (ISF; see Section 3.2) and the IASPEI Standard Seismic Phase List.

##### The ISC Bulletin

The main purpose of the ISC is to compile the ISC bulletin, regarded as the definitive record of the Earth's seismicity. Data is collected from over 130 agencies worldwide and is available online soon after being received. The reviewed ISC bulletin is typically available 24 months later and is manually checked by ISC analysts. In case sufficient data are available, events in the reviewed ISC bulletin are relocated using ISC's own location algorithm (ISCloc). Starting from 1900, the ISC bulletin contains a total of 12,095 events located within the "North Sea" area. It is useful to note that this number includes duplicates. As described in Section 4, these duplicates are identified and eliminated later.

#### 3.1.2 Germany

##### The BGR catalogue

The German Institute for Geosciences and Natural Resources ("Bundesanstalt für Geowissenschaften und Rohstoffe", BGR) is a German agency within the Federal Ministry of Economics and Technology. It acts as central geoscience consulting institution for the German federal government. Among other tasks, it generates the official German earthquake catalogue, including all analyses of federal German

station network operators with a prioritization of earthquake services (e.g., data from the German Regional Seismic Network - GRSN, the Saxonian and the Thuringian networks), now based on approximately 250 stations within Germany. However, events are not harmonized with catalogues of other seismic networks providers, e.g., the GEOFON and CAU catalogues (see below). We obtained the complete catalogue on personal request. This catalogue contains all events for which GRSN stations recorded analysable signals as well as the historical data from Leydecker (2011).

#### The GEOFON catalogue

The GEOFON programme resides at the German Research Centre for Geosciences, GFZ. It consists of a global seismic network (GE), a seismological data centre (GEOFON\_DC), a global EQ monitoring system (GEOFON EQinfo) and software development (amongst others SeisComp3). The GFZ Seismological Data Archive is the largest seismological data archive in Europe. Apart from the permanent GEOFON network, it holds data from 170 GEOFON partner networks with more than 5,700 stations as well as temporary station deployments (especially those of the GFZ Geophysical Instrument Pool and the German Task Force Earthquake) from 1993 to today. However, since we so far could not obtain phase readings, we will not consider events from the GEOFON catalogue in the rectangular North Sea catalogue.

#### The CAU catalogue

The Christian-Albrechts-University (CAU) in Kiel, Germany, operates a seismic network in cooperation with the State Geological Surveys of Schleswig-Holstein and Mecklenburg-Vorpommern. Densification of the previously sparse monitoring network, including installations on islands in the North and Baltic Sea, provide the basis for the creation of an independent event catalogue for the two northernmost German states and their adjacent seas. The catalogue was first published in 2019 and can be regarded as a link between the official German and Scandinavian earthquake catalogues, whose focuses are traditionally further south and north, respectively, away from the low seismicity area of the North German Basin. The Christian-Albrechts-University (CAU) is not a SHARP project partner, but a close collaboration has been established. Especially for events in recent years, previously unpublished waveform data from northernmost Germany, for example from the Helgoland array, is available.

### **3.1.3 The Netherlands**

Within the Netherlands, the Royal Netherlands Meteorological Institute (Koninklijk Nederlands Meteorologisch Instituut, KNMI) is responsible for the real-time determination of the epicentre, strength, and depth of both tectonic and induced seismic events, and the attribution of their causes. To this end data are acquired (monitoring using an extensive national seismic and acoustic network), interpreted (analysis and research) and distributed (data dissemination). The network maintained by the KNMI currently consists of 15 broadband seismometers, 99 borehole geophone stations, 97 accelerometers and 43 infrasound sensors.

#### The KNMI catalogue

The KNMI maintains its own catalogue, which is based on recordings by over 800 sensors. Not all of these sensors are still operational, and many of these sensors are borehole geophones, which are part of vertical strings of sensors (usually sampling the wavefield at the Earth's surface and depths of 50, 100, 150, and 200 m depth; Ruigrok & Dost, 2019). The KNMI network spans the whole of the Netherlands, but, due to the induced seismicity resulting from the gas extraction in the northern province of Groningen, station density is highest in and around that province. Starting from 1900, the

KNMI catalogue contained a total of 23 events that were located within the “North Sea” area.

### 3.1.4 The UK

The British Geological Survey (BGS) operates a national monitoring network across the UK to provide an immediate response to significant seismic events and to acquire seismic data on a long-term basis for understanding seismic hazard in the region. This network has evolved with time from the installation of the first stations in the late 1960's and currently consists of 50 broadband seismometers at stations across the UK along with 33 strong motion accelerometers with high dynamic range for recording strong signals. These data have been supplemented by various temporary deployments. As a result of these changes, the BGS earthquake catalogue is quite heterogeneous with a magnitude of completeness that varies in space and time. The current network is largely capable of detecting and locating all earthquakes with a magnitude of  $M_L \geq 2$  on mainland Britain, but this magnitude increases with distance offshore.

Prior to 1970, locations and magnitudes for events were estimated from macroseismic data from historical accounts of the impact of earthquake ground shaking on people and buildings. The estimated magnitude of completeness increases with time before present. Processing of instrumental data has changed with time, but in general, BGS combined automatic detection and location algorithms with manual review to provide phase picks, locations and magnitude estimates for all events. Focal mechanisms are calculated if data quality allows. This resulted in a catalogue of over 16,000 local events that includes natural and induced earthquakes as well as quarry blasts and other explosions. Many of these events are offshore and, where possible, BGS shared data with partner agencies in the region to try to improve location and magnitude estimates for these events.

### 3.1.5 Norway

Three different seismic event bulletins exist in Norway, i.e. the bulletin of the University of Bergen (UiB), the bulletin of NORSAR (NORSAR, 1971a) and the bulletin of the Norwegian National Seismic Network (NNSN, <https://nnsn.geo.uib.no>). The NNSN bulletin is compiled and maintained at UiB based on the two bulletins as well as analyst results stemming from both UiB and NORSAR. The Bergen bulletin contains entries for seismic events since the installation of the first seismic station in Bergen in 1905 as well as many historical events. The NORSAR bulletin for local and regional events starts in 1989. The NNSN bulletin should contain all information from the other two bulletins, but unfortunately this is not always the case. In particular, the array analysis results (back-azimuth and slowness estimates of the seismic onsets) from the different NORSAR arrays often is missing. In addition, because of the online data exchange between UiB's and NORSAR's (NORSAR, 1971b) networks, many onsets were read and analysed at both institutes with slightly different results and UiB included only one of these readings in the NNSN bulletin. Therefore, we retrieved both - the complete NNSN bulletin from UiB and the complete NORSAR bulletin - for all events within the rectangular area of interest and handle them as individual entries. Any double entries regarding events or onsets will be removed when joining the bulletin information with the other sources.

### 3.1.6 Denmark

The Geological Survey of Denmark and Greenland (GEUS) is the National Data Centre and responsible for the seismic service for Denmark and Greenland (denoted by DNK in the bulletin). Data are streamed in real-time from stations in both Denmark and Greenland and are monitored for tectonic and non-tectonic events. In Greenland, this includes cryoseismic events as well as landslides. In Denmark, the non-tectonic events are primarily explosions. GEUS operates eight long-term stations as well as a varying number of short-term stations in Denmark, all of which constitute broadband stations, one of which is a borehole installation. In the monitoring process GEUS also utilizes data from neighboring countries, primarily Sweden and Norway, which greatly improves the ability to detect and locate events.

GEUS maintains its own catalogue based on the DNK network in Denmark and the virtual network GLISN in Greenland ([www.glisn.info](http://www.glisn.info)), which includes both stations in the DNK network as well as other networks. Events located by the Norwegian and Swedish networks (NNSN and SNSN) in the area close to Denmark are merged into the GEUS catalogue. For the SHARP project, events were extracted from this catalogue.

### 3.2 Format

The IASPEI Seismic Format (ISF) is used as one of the standards to share data with the International Seismological Centre (ISC) and other seismological organisations. A seismological bulletin in ISF format consists of lists of events with corresponding information on origins, magnitudes, phase arrivals, stored in the form of blocks (International Seismological Centre, <http://www.isc.ac.uk/standards/isf>). A single event contains an event title, origin block, magnitude, and phase sub-blocks. Additional information on moment tensors, fault plane solutions, comments etc., can also be included. Each sub-block starts with a header line, followed by the data lines. The structure is based on strict character writing within the set range of bytes within each block. An example of the file structure for an individual event in the North Sea is shown in Figure 3.1.

### SHARP Storage – Project no 327342

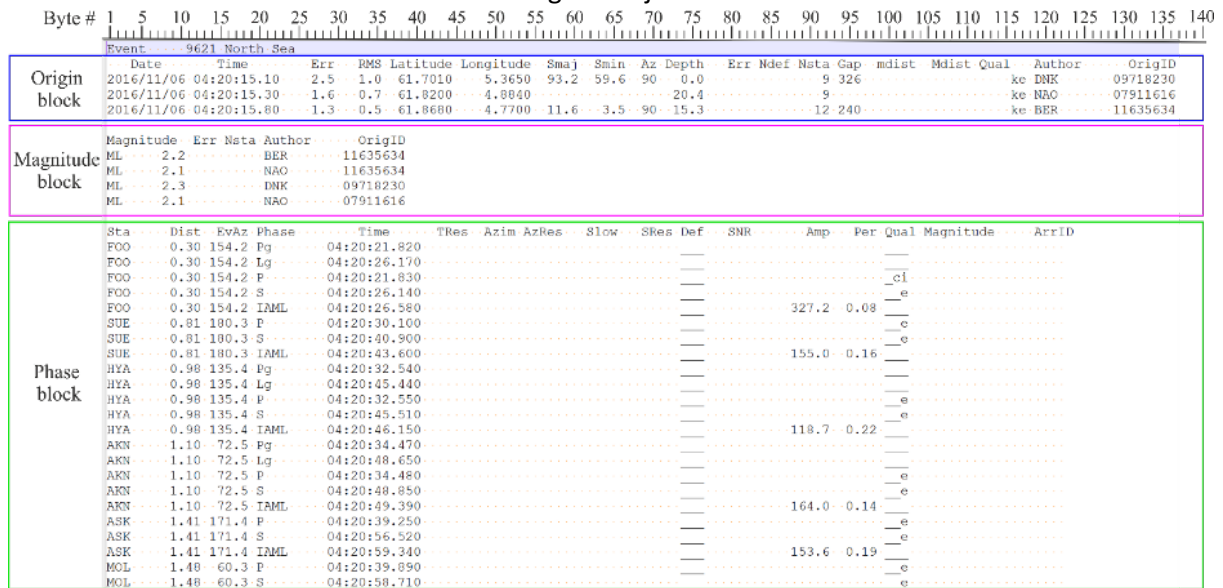


Figure 3.1: Example of the .isf file structure using an event within the North Sea.

The origin block consists of a header line (Figure 3.1, blue rectangle) and the following data block with character placement for 24 parameters. The structure of this block is described in Table 1.

Header name	Bytes	Format	Description
Date	1-10	i4,a1,i2,a1,i2	epicentre date (yyyy/mm/dd)
Time	12-22	i2,a1,i2,a1,f5.2	epicentre time (hh:mm:ss.ss)
	23	a1	fixed flag (f = fixed origin time solution, blank if not a fixed origin time)
Err	25-29	f5.2	origin time error (seconds; blank if fixed origin time)
RMS	31-35	f5.2	root mean square of time residuals (seconds)
Latitude	37-44	f8.4	latitude (negative for South)
Longitude	46-54	f9.4	longitude (negative for West)
	55	a1	fixed flag (f = fixed epicentre solution, blank if not a fixed epicentre solution)
Smaj	56-60	f5.1	semi-major axis of 90% ellipse or its estimate (km, blank if fixed epicentre)
Smin	62-66	f5.1	semi-minor axis of 90% ellipse or its estimate (km, blank if fixed epicentre)

Az	68-70	i3	strike ( $0 \leq x \leq 360$ ) of error ellipse clockwise from North (degrees)
Depth	72-76	f5.1	depth (km)
	77	a1	fixed flag (f = fixed depth solution, d = depth phases, blank if not a fixed depth)
Err	79-82	f4.1	depth error 90% (km; blank if fixed depth)
Ndef	84-87	i4	number of defining phases
Nst	89-92	i4	number of defining stations
Gap	94-96	i3	gap in azimuth coverage (degrees)
mdist	98-103	f6.2	distance to closest station (degrees)
Mdist	105-110	f6.2	distance to furthest station (degrees)
Qual	112	a1	analysis type: (a = automatic, m = manual, g = guess)
Qual	114	a1	location method: (l = inversion, p = pattern recognition, g = ground truth, o = other)
Qual	116-117	a2	event type
Author	119-127	a9	author of the origin
OrigID	129-136	a8	origin identification

Table 3.1: Origin block description.

The origin block is followed by information on magnitudes (Figure 3.1, magenta rectangle). The following seven parameter names are used for the magnitude block:

Header name	Bytes	Format	Description
Magnitude	1-5	a5	magnitude type (mb, Ms, ML, mbmle, msmle)
	6	a1	min max indicator (<, >, or blank)
	7-10	f4.1	magnitude value
Err	12-14	f3.1	standard magnitude error
Nsta	16-19	i4	number of stations used to calculate magnitude

Author	21-29	a9	author of the origin
OrigID	31-38	a8	origin identification

Table 3.2: Magnitude block description.

The phase block comes after the magnitudes data section (Figure 3.1, green rectangle). Twenty-three parameters are coded using the following convention:

Header name	Bytes	Format	Description
Sta	1-10	1-5	station code
Dist	12-22	7-12	station-to-event distance (degrees)
EvAz	23	14-18	event-to-station azimuth (degrees)
Phase	25-29	20-27	phase code
Time	31-35	29-40	arrival time (hh:mm:ss.sss)
TRes	37-44	42-46	time residual (seconds)
Azim	46-54	48-52	observed azimuth (degrees)
AzRes	55	54-58	azimuth residual (degrees)
Slow	56-60	60-65	observed slowness (seconds/degree)
SRes	62-66	67-72	slowness residual (seconds/degree)
Def	68-70	74	time defining flag (T or _)
	72-76	75	azimuth defining flag (A or _)
	77	76	slowness defining flag (S or _)
SNR	79-82	78-82	signal-to-noise ratio
Amp	84-87	84-92	amplitude (nanometres)
Per	89-92	94-98	period (seconds)
Qual	94-96	100	type of pick (a = automatic, m = manual)
	98-103	101	direction of short period motion (c = compression, d = dilatation, _ = null)
	105-110	102	onset quality (i = impulsive, e = emergent, q = questionable, _ = null)
Magnitude	112	104-108	magnitude type (mb, Ms, ML, mbmle, msmle)
	114	109	min max indicator (<, >, or blank)

	116-117	110-113	magnitude value
ArrID	119-127	115-122	arrival identification

Table 3.3: Phase block description.

### 3.3 Rectangular bulletin

The rectangular bulletin consists of the input from the Institute for Geosciences and Natural Resources (BGR), British Geological Surveys (BGS), Geological Survey of Denmark and Greenland (GEUS), the International Seismological Centre (ISC), the Royal Dutch Meteorological Institute (KNMI), Norwegian National Seismic Network (NNSN), and Norwegian Seismic Array (Norsar). At this stage, the database in IASPEI Seismic Format (ISF) contains 51,634 events detected between 1382 and 2022 (Figure 3.2). The selection of events for the rectangular bulletin is based on a rectangular area of interest bounded by latitudes of 50° and 62.5° North and longitudes of 7.5° west and 12.5° East. The bulletin contains information on earthquake origins, interpreted phases and, in some cases, focal mechanisms within the region of interest. The rectangular bulletin has a significant number of events onshore adjacent to the North Sea and event or origin duplicates. Therefore, the processing steps described in Section 4 involved excluding the events outside of the polygon bounding the area of interest (green polygon, Figure 3.2), event association, and cleaning of the ISF bulletins.

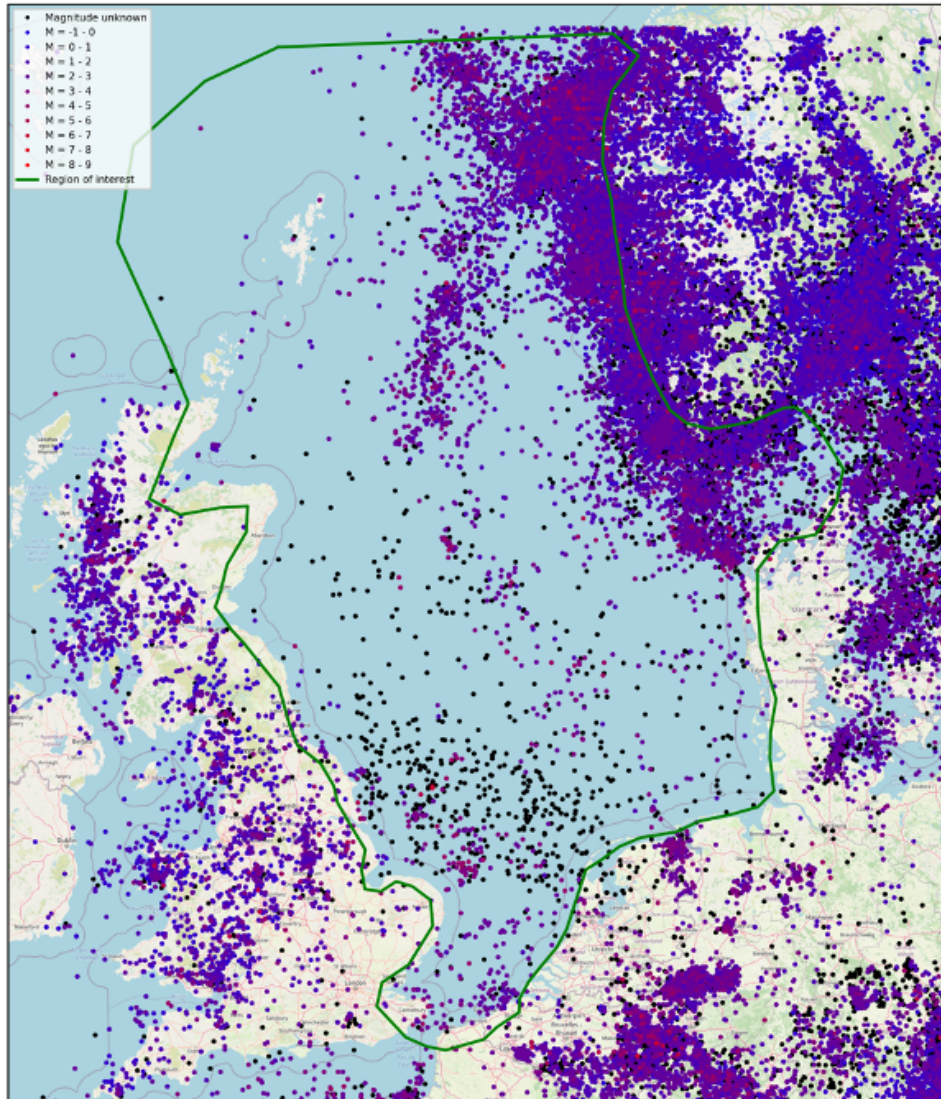


Figure 3.2: Event distribution (solid dots) of the rectangular North Sea bulletin. Colours indicate the estimated magnitudes. Black implies no magnitude estimate was available.

## 4. North Sea Bulletin

In this section, we describe the different steps and decisions leading to the delivered North Sea catalogue (i.e., D2.1). We first describe the determination of the area of interest (Section 4.1), which is demarcated by the polygon in Figure 3.2. In Section 4.2, we describe how we move from the rectangular catalogue to a catalogue containing only the events within the area of interest. This includes the removal of origins that are obviously erroneous. The subsequent event association, which identifies and eliminates duplicate events, reduces the number of events by approximately 50%. This is explained in detail in Section 4.3. It results in the North Sea catalogue delivered here. In the next two years, this catalogue will be updated and augmented with more event data and focal mechanisms (resulting in deliverable 2.4). Finally, the results of a preliminary statistical analysis of the delivered catalogue are presented in Section 4.4.

For clarity, we repeat here the definition of the terms "catalogue" and "bulletin": "catalogue" refers to the simpler lists of unique events, each with a single origin time, location, and magnitude; while "bulletin" refers to the more complete data set, where each event can have several measured origin times and locations, and phase readings are included. Generally speaking, "catalogues" are produced from the bulletins, with each event in the catalogue being the "prime" entry in the bulletin. The distinction between "events" and "entries" in the ISC format should also be clarified here: an "event" refers to a set of collected origins, magnitudes and phases, whilst an "entry" refers to a single line of data within the origin, magnitude, or phase blocks (see Section 3.2).

### 4.1 Determination of the polygon

A detailed polygon was chosen to capture only those events within the North Sea. The shape of this polygon is largely determined by the coastlines to the East, South and West, however, we extend the polygon inland by approximately 10 km to ensure that we capture any events that may have been mislocated onshore. To the North, we extend the polygon to a latitude of 62.5° North to adequately capture seismicity in the Viking Graben. Similarly, we extend the polygon into the Skagerrak strait to capture seismicity between Denmark and Norway. The polygon extends to the continental shelf west of the Shetland Isles.

### 4.2 Event selection

The first stage of event selection is the application of the polygon described above. This would represent a simple spatial filter; however, each event can have several origins from different reporting agencies. This means that for an individual event, some origin locations may fall within the polygon, while others may be outside of it. We removed events for which all origin locations are outside the polygon, and kept only events for which at least one origin location is situated within the polygon. However, a few events contained origin locations at very large distance from the polygon, indicating that the associated entry in the origin block might be anomalous. Each event containing an origin location more than 100 km from the edge of the polygon was therefore manually reviewed.

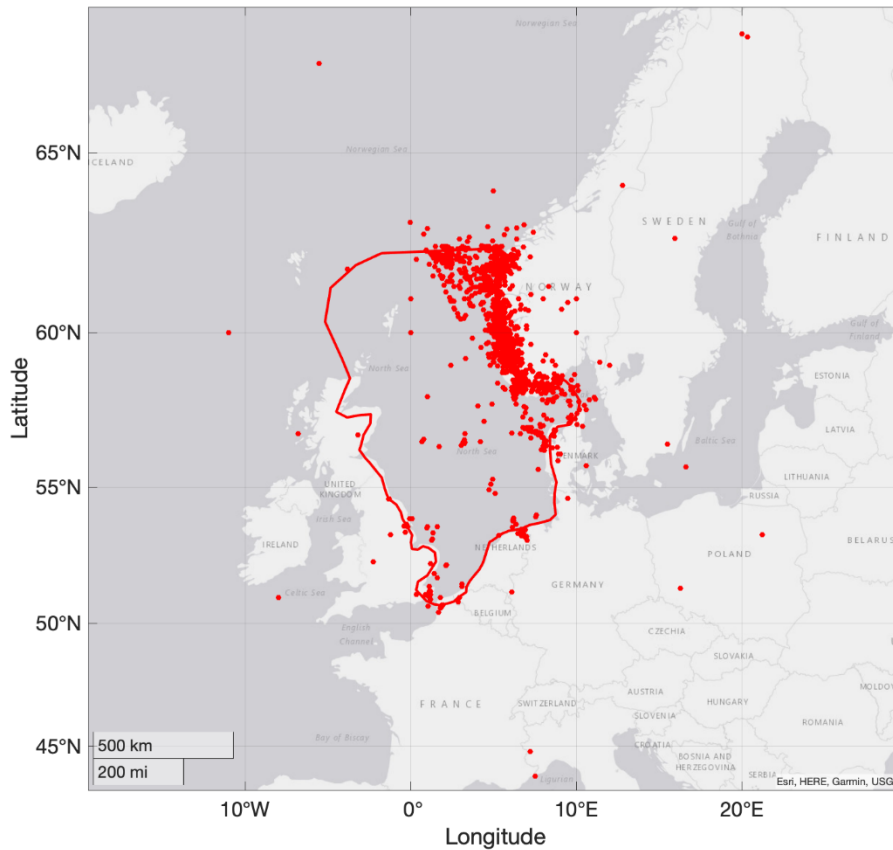


*Figure 4.1: Map showing the initial results of events with at least one origin location that is outside the polygon. All origin locations are depicted as red dots.*

The manual inspection revealed several erroneous origins or entries within event origin blocks. These are evident in Figure 4.1, sometimes thousands of kilometres from the study region. This is most likely the result of incorrect association of events in the underlying bulletins, where a random earthquake (potentially with a similar origin time) had been grouped in with an entirely different event. Origins that are clearly erroneous were therefore manually removed. Predominantly, these erroneous origins were present in events from the ISC bulletin and will be reported back to the ISC. The events that still contain at least a single origin location outside of the polygon remaining in the bulletin after this step are shown in Figure 4.2. Note that this work step did not reduce the overall number of events, as only origin block entries were removed.

We chose not to remove events based on their entry’s listed “event type” at this stage. This is because most events are not labelled, and because other events contain entries with conflicting labels, e.g., labelled as earthquake by one agency and as explosion by. Event types will be investigated further during the reprocessing of the bulletin.

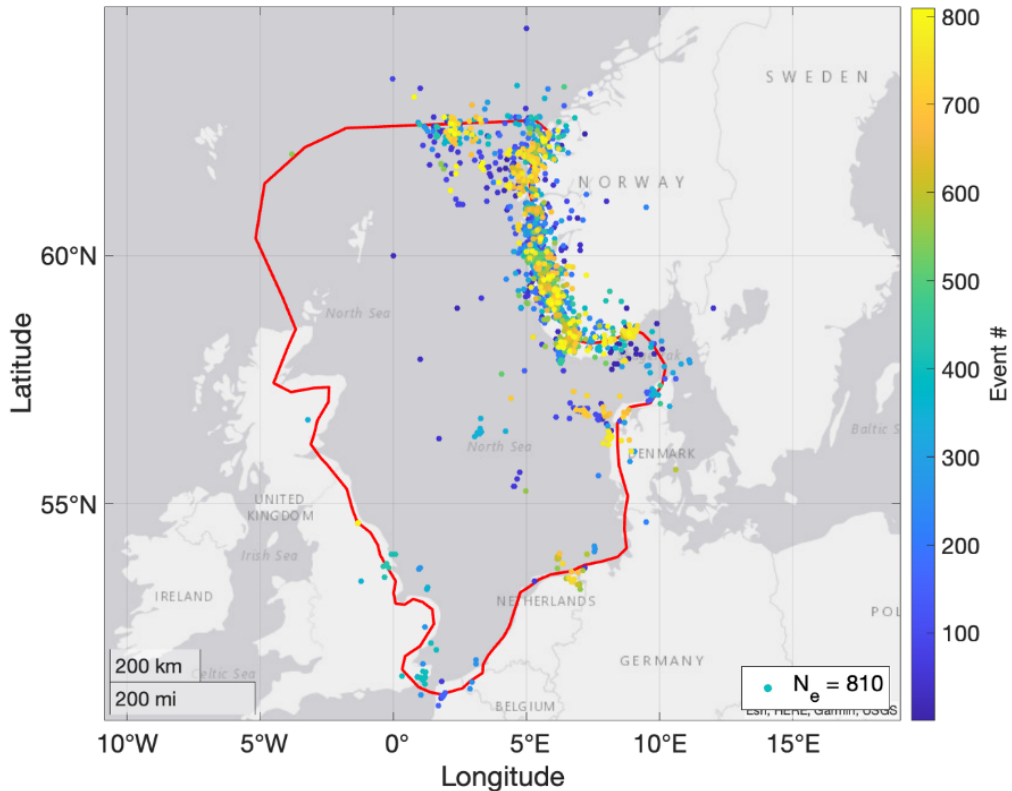


Figure 4.2: Map showing the remaining origin locations associated with events containing at least one origin with a location outside of the polygon after manually removing anomalous origins. Origin locations are coloured by event number.

### 4.3 Bulletin merging and event association

All of the agencies' bulletins were merged to form a single database, to which the polygon described above was applied. The results are shown in Figure 4.3. After the manual elimination of obviously erroneously entries (see Section 4.2), events were associated with each other and potentially merged. This is the primary and most significant step of the merging of the bulletins. Here, data blocks that appear to concern the same event, but are present as separate events reported by different agencies, are merged into a single event in the file.

Although it is not strictly used in the event association, an important step prior to this event association is the assignment of unique origin block entry identifiers ("OrigIDs"). Each origin in the merged, non-associated bulletin is given a unique OrigID, which is in the form of a 6-digit number. The first digit of this number corresponds to the agency from which the entry originated. These are 1=BGR, 2=BGS, 3=GEUS, 4=ISC, 5=KNMI, 6=NNSN, and 7=NORSAR. The OrigID is repeated in the magnitude block, corresponding to the associated entry in the origin block, and also used in the arrival identifier (the "ArrID") in the phase block. For the ArrID, the OrigID of the prime entry in the origin block is prepended to the number of its position in the phase block. This ensures each ArrID remains unique. Due to the character limit for OrigIDs and ArrIDs in the ISC format, the OrigID and the position within the phase must be encoded in a denser format. We use hexadecimal encoding for this purpose. An example event from the bulletin is shown in Figure 4.4.

After the assignment of OrigIDs, additional phase and origin data for 9 events were provided by the University of Kiel (CAU catalogue, Section 3.1.2) and manually added to the bulletin file. This data has a different format of OrigID and ArrID: the Author “UNIK” is given to each of the origin block entries, along with the OrigID “UNIK” followed by the number 1 through 9. As before, the ArrIDs for the Kiel data are the OrigID appended with an underscore followed by a sequentially increasing two-digit number.

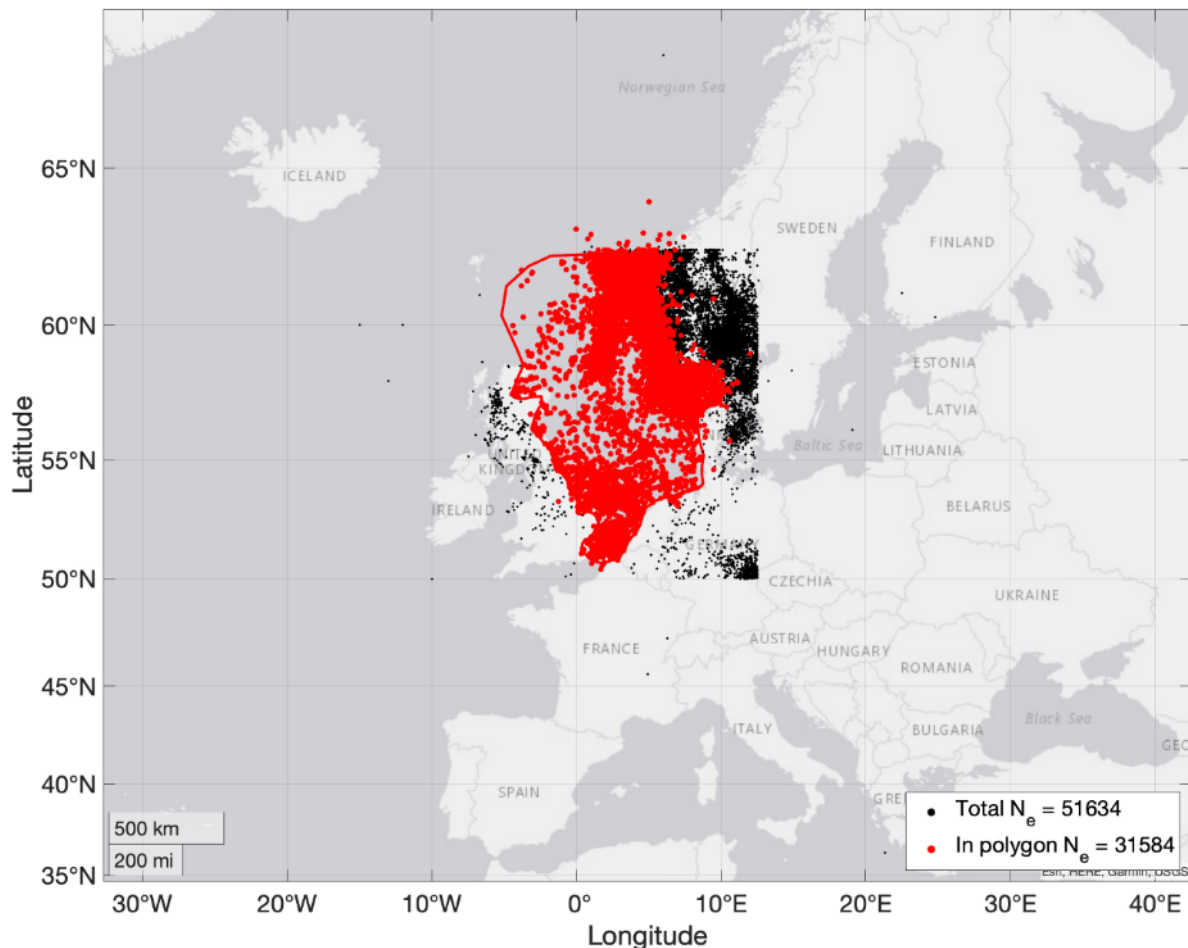


Figure 4.3: Map of events included in the first stage of bulletin merging. Black dots show origins from the bulletins provided by the individual agencies, which include origin locations from the larger, rectangular search area. Red dots show the locations of the origins remaining after the application of the polygon and subsequent cleaning steps.

A simple yet widely used method (Jones et al., 2000; Jónasson et al., 2021) is used to associate events. The origin times and locations of all origins are compared, and if they are similar within a predefined threshold, the origin, magnitude, and phase blocks are merged and treated as a single event. This algorithm first extracts all origin times and locations from the origin block for each event. It then loops through each origin time and location and compares it to all others in the bulletin. If the difference in time is less than 30 s and the location difference is less than 1°, the data are grouped into a single event. For a small number (2.5%) of the 43,718 entries, there are no locations given. In these cases, we just apply the time association threshold. Once associated, the entries are grouped and merged to form a new “matched”, event associated bulletin. Whilst this algorithm takes into account all origin

data, propagating through each entry in the origin blocks of all events, it can lead to duplication of origin and phase data in the event merging process. There are 31,258 events in the initial merged, unassociated bulletin file. This initial merging algorithm reduces the number of events in the file to 15,850.

Event	31252 North Sea													Author	OrigID			
Date	Time	Err	RMS	Latitude	Longitude	Smaj	Smin	Az	Depth	Err	Ndef	Nsta	Gap	mdist	Mdist	Qual	Author	OrigID
2022/06/21	15:56:20.30	0.20	0.80	58.2780	0.9090				119.6	173	3						ke DNK	67736
2022/06/21	15:56:22.24	2.60	0.80	59.3483	1.1405	82.0	40.0	161	0.0f	9		215	4.65	12.48		ke NAO	666F8	
2022/06/21	15:56:22.90	1.30	0.50	59.1410	1.3350	5.0	3.9	90	6.2			21	99			ke BGS	65B05	
2022/06/21	15:56:24.30	1.40	0.50	59.1540	1.3210	4.0	3.0	90	16.3			24	102			ke BER	70DEB	

Magnitude	Err	Nsta	Author	OrigID
ML	2.3		BER	70DEB
mb	3.7		NAO	666F8
ML	2.7		BGS	65B05

Sta	Dist	EvAz	Phase	Time	TRes	Azim	AzRes	Slow	SRes	Def	SNR	Amp	Per	Qual	Magnitude	ArrID
LRW	1.61	308.9	P	15:56:50.940												67736 1
LRW	1.61	308.9	S	15:57:10.480												67736 2
LRW	1.61	308.9	IAML	15:57:15.250								69.9	0.36			67736 3
LRW	1.61	308.9	P	15:56:50.890												67736 4
LRW	1.61	308.9	S	15:57:10.390												67736 5
LRW	1.61	308.9	IAML	15:57:13.280								109.7	0.32			67736 6
LRW	1.61	308.9	IAML	15:57:14.570								73.2	0.37			67736 7
KMY	2.02	86.7	P	15:56:56.800												67736 8
KMY	2.02	86.7	S	15:57:20.780												67736 9
KMY	2.02	86.7	IAML	15:57:26.920								85.8	0.29			67736 A
KMY	2.02	86.7	Pn	15:56:56.130												67736 B
KMY	2.02	86.7	Sn	15:57:21.400												67736 C
KMY	2.02	86.7	P	15:56:55.910												67736 D
KMY	2.02	86.7	S	15:57:20.590												67736 E
KMY	2.02	86.7	IAML	15:57:30.700								47.2	0.16			67736 F
KMY	2.02	86.7	IAML	15:57:30.840								74.2	0.42			67736 10
STAV	2.27	93.7	P	15:57:00.470												67736 11
STAV	2.27	93.7	Pn	15:57:00.700												67736 12
STAV	2.27	93.7	Sn	15:57:26.790												67736 13
ASK	2.37	54.1	P	15:57:00.320												67736 14
ASK	2.37	54.1	S	15:57:26.690												67736 15
ASK	2.37	54.1	IAML	15:57:39.900								38.1	0.30			67736 16
ASK	2.37	54.1	Pn	15:57:00.340												67736 17
ASK	2.37	54.1	Sn	15:57:27.650												67736 18
BER	2.38	57.0	P	15:57:00.540												67736 19
BER	2.38	57.0	S	15:57:27.900												67736 1A
BER	2.38	57.0	IAML	15:57:37.700								36.3	0.32			67736 1B
BER	2.38	57.0	Pn	15:57:00.550												67736 1C
BER	2.38	57.0	Sn	15:57:27.140												67736 1D

Figure 4.4: An example event in the bulletin.

Further, the bulletin is put through a second round of event association and cleaning, removing duplicate events and repeated origins. The first of these steps is to identify events with very similar (<1 s difference) origin times in the prime entry. The algorithm first checks each of these cases for a complete repetition of the same data and removes the repeated event if appropriate. If the two events with similar prime origin times contain different data, the two events are merged. This process brought the event number in the bulletin to 15,351, and thus accounted for the removal of 499 duplicated events. This algorithm has the potential to introduce a small number of repeated entries in the origin block, though this is dealt with in the subsequent cleaning step.

This step involves comparing the OrigIDs both within and between events. As each entry has a unique OrigID, a simple way to remove duplicate events and entries introduced in the merging process is to look for repeated OrigIDs. The algorithm first looks within each event, and removes duplicated entries, i.e., those with the same OrigID. The next step searches for OrigIDs duplicated between different events. If the data is wholly replicated in either of the events, the repeated data is deleted. If the data is not wholly repeated, the two events are merged. A second removal of repeated data within each event is performed subsequently. This process removed another 40 events from the bulletin and several hundred repeated lines in the origin blocks, bringing the final event total to 15,311 (Figure 4.5).

A final cleaning of the bulletin is conducted to remove identical lines in the magnitude and phase blocks, which also removes lines which are *functionally* identical. The algorithm first checks for entirely repeated lines and removes them. The ArrID for the deleted lines is preserved and appended onto the

phase block entry that is kept. Comparisons are then made between different phase block entries, identifying entries for which the name of the phase is functionally identical. This final cleaning step removed another 1630 lines from the ISF file but does not remove entire events.

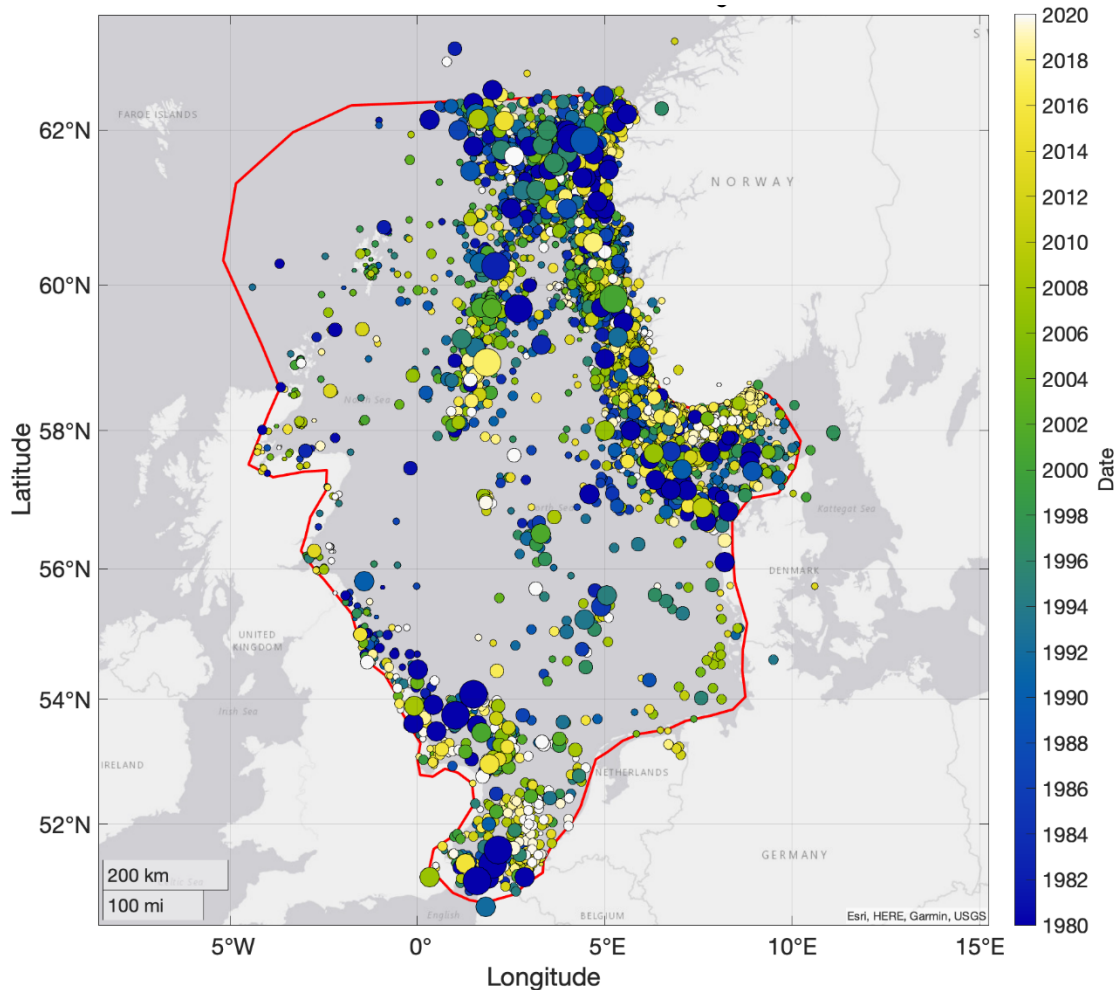


Figure 4.5: Map showing the locations of bulletin prime origins in the merged, event associated, and cleaned data. Epicentral locations (circles) coloured by year of occurrence.

#### 4.4 Preliminary statistical analysis

The event associated bulletin consists of 15,311 events and 43,730 origin block entries. Figure 4.5 shows the locations and magnitudes of the prime entries in the bulletin, i.e., the catalogue. Patterns in seismicity rates and detection thresholds are clear. Higher rates of seismicity are evident in the Viking graben region, and – due to historically dense coverage and more recent advances in monitoring in Norway – detection rates within 100-200 km of the Norwegian coast are high.

Figure 4.6 shows the number of events from each of the agencies. This generally reflects the fact that the Norwegian, UK, and Danish agencies have the better detection capability for North Sea seismicity, and that the ISC data is the amalgamation of each of the agencies’ catalogues.

SHARP Storage – Project no 327342

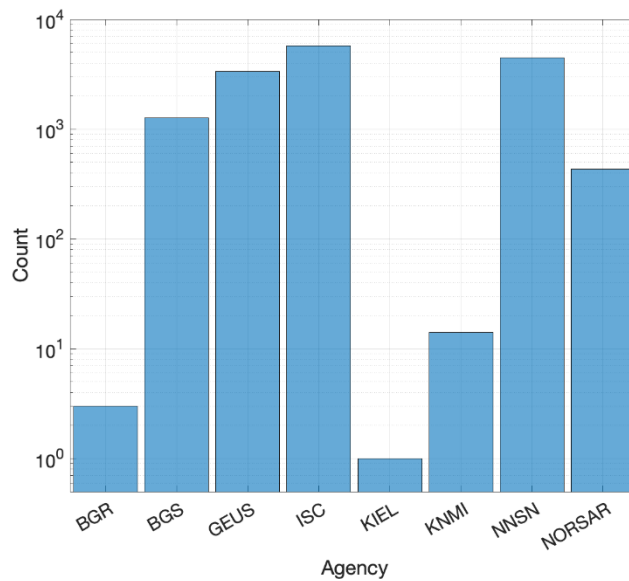


Figure 4.6: Histogram showing the number of events from each agency in the prime entries of the merged bulletin.

Figure 4.7 shows the histogram of listed event types. Only around 10% of the entries are classified, making the assessment of the distribution for the whole bulletin difficult. The majority are suspected or known explosions (“sh” or “kh” in ISF formatting), though it is unlikely to be reflective of the entire bulletin. Suspected and known earthquakes seem to make up a minority of the event data, though this is most likely a result of the agencies not reporting event types in the ISF format files. In addition, the label “M” appears to have been used for a small number of events by some agencies, but its meaning is unclear. These will be treated as “unknown” type events going forward.

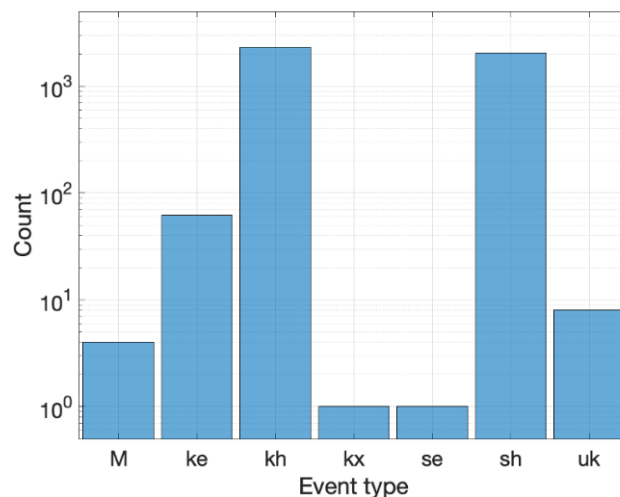


Figure 4.7: Event type histogram for entries in the bulletin. Those in lowercase follow the standard formatting of ISF, with: “s” denoting suspected; “k” denoting known; “e” denoting earthquake; “h” denoting an explosion; and “uk” denoting an unknown origin. Meaning of “M” unclear.

One can observe the temporal changes in magnitude of completeness  $M_c$  clearly in Figure 4.8. This  $M_c$  refers to the magnitude of events for which all events larger than that have been detected and reported. This will vary both in time and in space, reflecting the limited coverage of sensors in the middle of the North Sea compared to its coasts. Having spatiotemporal variations in  $M_c$  can introduce

significant complexity in examining earthquake statistics and seismic hazard, and will be accounted for in future work.

Prior to approximately 1980, events with  $M_L < 4$  were not routinely detected. From 1985, smaller events with  $M_L < 3$  are detected and reported far more often. Magnitude of completeness will also vary dramatically in different regions of the study area. Though thorough completeness analysis will be undertaken in future work, a reasonable estimate would be that the catalogue is complete from  $M_L > 4$  in the past several decades. This also does not account for the differences in the measurement of  $M_L$  in the different jurisdictions within the study region. Magnitude homogenisation will be addressed in future further analysis, and its result published in deliverable 2.4 (see Section 1.1).

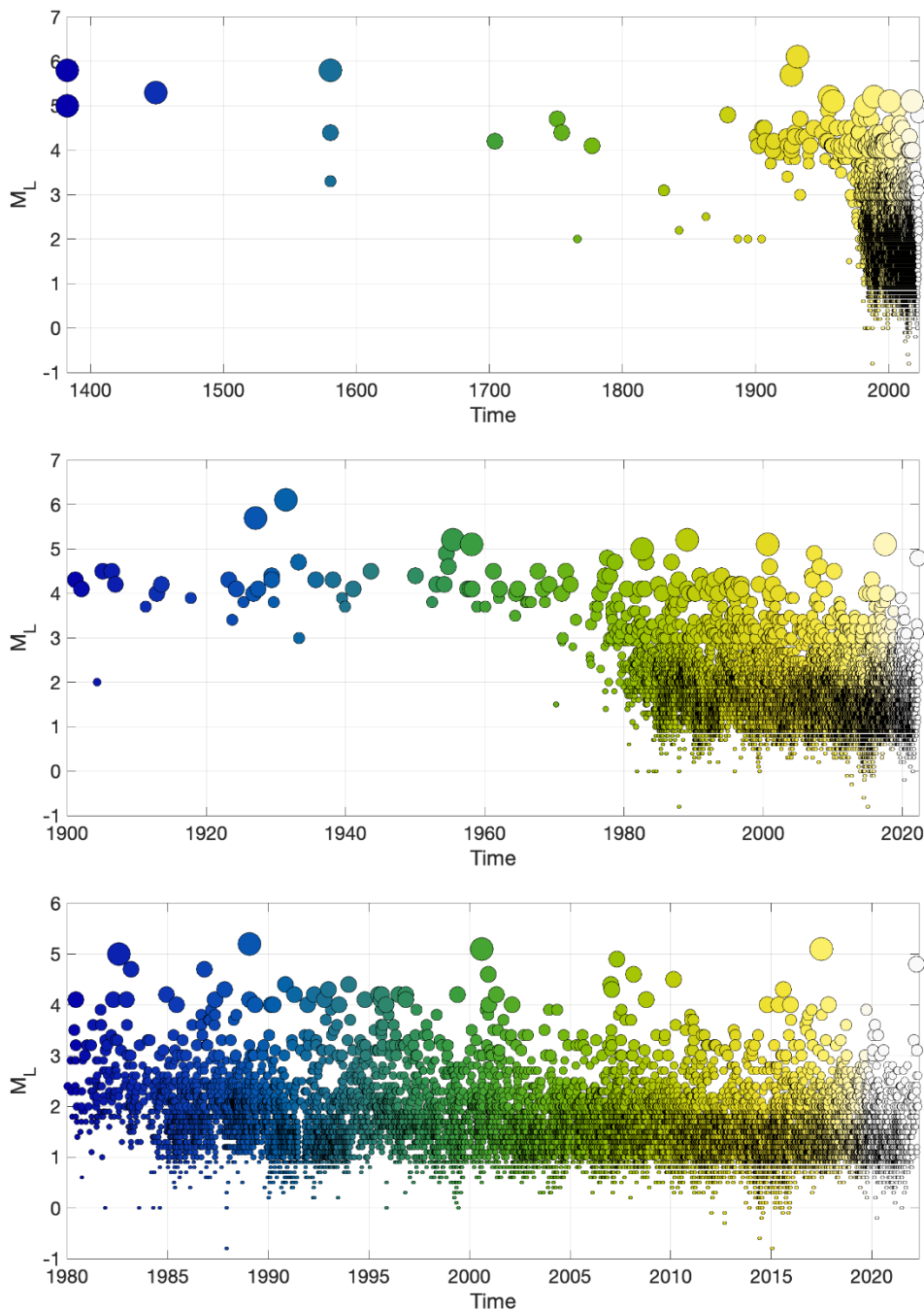


Figure 4.8: Local magnitude of prime origins of events through different time periods. The top figure starts from the earliest events in the catalogue (May 1382). The middle shows from 1900, when instrumental measurements of earthquakes began in earnest in the region. The bottom figure presents events only after 1980, when earthquake detection improved to routinely detect  $M > 3$  events.

With the caveat of the magnitudes in the catalogue being not homogenised, at least a preliminary magnitude distribution can be analysed. The local magnitude-frequency distribution is shown in Figures 4.9 and 4.10, along with the measured Gutenberg-Richter (GR) b-value. This empirical GR relationship relates the number of events  $N$  to the magnitude  $M$ , with  $b$  characterising the slope of the line in log space, and the overall activity rate given by  $a$ :

$$\log(N) = a - bM$$

We calculate the b-value using the maximum likelihood approach of Aki (1965), with updated uncertainty estimates of Tinti & Mulargia (1987; see Marzocchi & Sandri, 2003). We first find the magnitude of completeness  $M_{\min}$  using the b-value stability method of Cao & Gao (2002), and then follow the procedure of Roberts et al. (2015). This produces the notably low b-value of  $0.8 \pm 0.02$  shown in Figure 4.9. Though this represents a stable b-value,  $M_{\min}$  is most likely largely underestimated and thus results in a corresponding small uncertainty in the b-value. Instead, we decided to impose a more realistic  $M_{\min}$ , producing the b-value measurement shown in Figure 4.10.

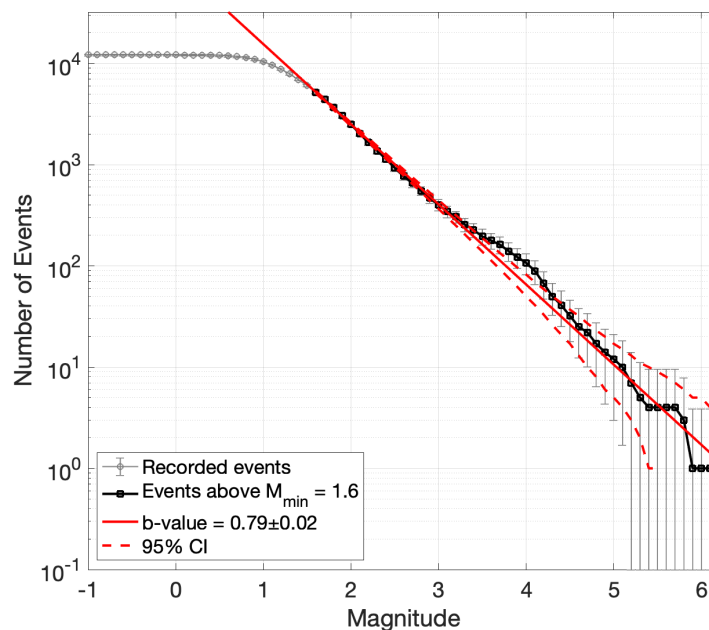


Figure 4.9: The magnitude-frequency distribution for the catalogue using local magnitude  $M_L$ .

The resulting b-value ( $1.0 \pm 0.2$ ) is much closer to what is expected in tectonic settings (b of around 1). Figure 4.10 also more clearly shows an unexpected oscillation in the magnitude frequency distribution between  $2 < M_L < 4$ . This could result from the variation in completeness magnitude through space and time in the catalogue, or the differing magnitude scales used by the contributing agencies. If small events ( $M < 4$ ) are underreported in the catalogue relative to the larger events ( $M > 4$ ), which is likely, this would give an underestimate in the number of small events, resulting in a decrease of the measured b-value. Depending on the underlying magnitude scale, local magnitude can systematically underestimate the magnitude of small ( $M < 3$ ) events (Deichmann, 2017). This could also result in the

lower b-value observed for lower magnitudes. This difference will be more thoroughly investigated in a future study of the catalogue.

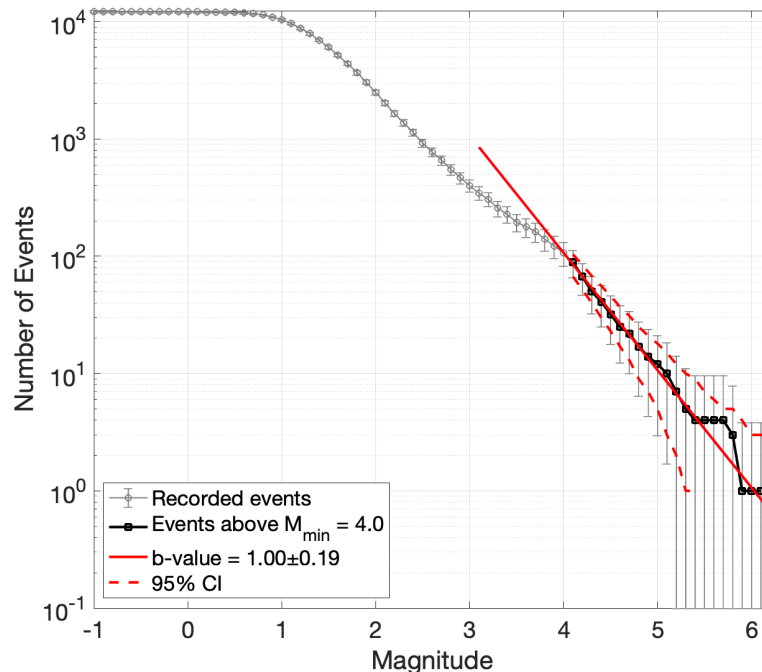


Figure 4.10: The magnitude-frequency distribution for the prime entries in the bulletin using local magnitude  $M_L$ . GR b-value was calculated with a more realistic estimate of magnitude of completeness  $M_{min}$ :  $M_L = 4$ .

## 4.5 Focal mechanism catalogue

In addition to the bulletin described in the previous sections, we collected information to provide a catalogue of computed focal mechanisms for the same region. Since this catalogue will be used for interpretation of the stress field, only high-quality data should be included. Therefore, we restricted the catalogue to events after 1980 (starting with the year 1981), at which point the detection threshold in the North Sea had sunk considerably. So far, focal mechanism catalogues were collected from the following providers:

- the Harvard CMT/GCMT catalogue (downloaded from: <https://www.globalcmt.org/CMTsearch.html>; Dziewonski et al., 1981; Ekström et al., 2012);
- the ISC focal mechanism bulletin (downloaded from: <http://www.isc.ac.uk/iscbulletin/search/fmechanisms/>; ISC, 2022; Lentas, 2018; Lentas et al., 2019);
- the GEOFON moment tensor catalogue (downloaded from: <https://geofon.gfz-potsdam.de/old/eqinfo/form.php>; Quinteros et al., 2021)
- focal mechanism catalogues of countries bordering the North Sea:
  - GEUS, Denmark (see section 3.1.6 for details);
  - Norwegian National Seismic Network (NNSN, <https://nnsn.geo.uib.no>), Norway. Since mechanisms may considerably vary in quality, only reviewed mechanisms published in

Tjåland & Ottemöller (2018) were considered for now. A further collection by Tjåland (2020) only contains solutions of C and D quality, which were disregarded for now.

In addition, catalogues from the following sources were checked, but did not record any focal mechanisms for events in the study area:

- KNMI (see Section 3.1.3 for details);
- NORSAR (see Section 3.1.5 for details);
- BGR, Germany (see Section 3.1.2 for details);
- Christian-Albrechts-University (CAU) in Kiel, Germany (see Section 3.1.2 for details);
- World Stress Map database (accessed via <https://www.world-stress-map.org/casmo>; Heidbach et al., 2016), mechanisms of quality assessed as “A” or “B”.

Focal mechanisms from the following sources may be added in the future:

- BGS, United Kingdom (see section 3.1.5 for details);
- further mechanisms extracted from the NNSN catalogue;
- literature.

The following work steps were integrated:

- Magnitudes from the catalogue described in sections 4.2 to 4.4 were added to the following events within the ISC focal mechanism catalogue, since they were missing:
  - 22.05.2015, author ISC: use Mw=4.5 from author STR;
  - 22.05.2015, author NEIC: use Mw=4.5 from author STR;
  - 25.06.2017, author BER: use ML=2.6 from BER;
  - 30.06.2017, author ISC: use Mw=4.8 from GCMT;
  - 09.06.2018, author BGS: use ML=4.1 from BGS;
  - 12.06.2019, author BER: use ML=1.9 from BER;
  - 21.09.2019, author BER: use ML=1.2 from BER;
  - 23.01.2020, author BGS: use ML=3.1 from BGS.
- Double entries were removed, if they were reported by the ISC as well as the primary author. This concerns the following entries in the ISC catalogue:
  - removed 30.06.2017 13:33:47 as reported by ISC with author GCMT, since reported within GCMT catalogue as well;
  - removed 09.10.2016 12:48:30 as reported by ISC with author GCMT, since reported within GCMT catalogue as well (although strike 1/2, dip 1/2, rake 1/2 interchanged);
  - removed 07.01.2007 01:50:57 as reported by ISC with author GCMT, since reported within GCMT catalogue as well (although strike 1/2, dip 1/2, rake 1/2 interchanged);
  - removed 01.11.2004 22:26:59 as reported by ISC with author Bergen, since reported within NNSN catalogue as well (but with ML instead of Mw, although same value); however, overtook timing from ISC, since seconds are truncated in NNSN reviewed catalogue as reported by Tjåland & Ottemöller (2018);
  - adopted timing of 12.08.2000 14:27:26 event from ISC catalogue with author Bergen to NNSN entry (see above), but left both entries, since mechanism potentially different.
- If several entries exist for the same event, entries were sorted using the following hierarchy:
  - GCMT;
  - NEIC;

- ISC;
- GEUS;
- BGS;
- NNSN;
- BER;
- GEOFON;
- MED\_RCMT.

The resulting focal mechanism catalogue contains 60 entries describing presumably 50 individual events. It is available as file accompanying this report and illustrated in Figure 4.11 and Figure 4.12.

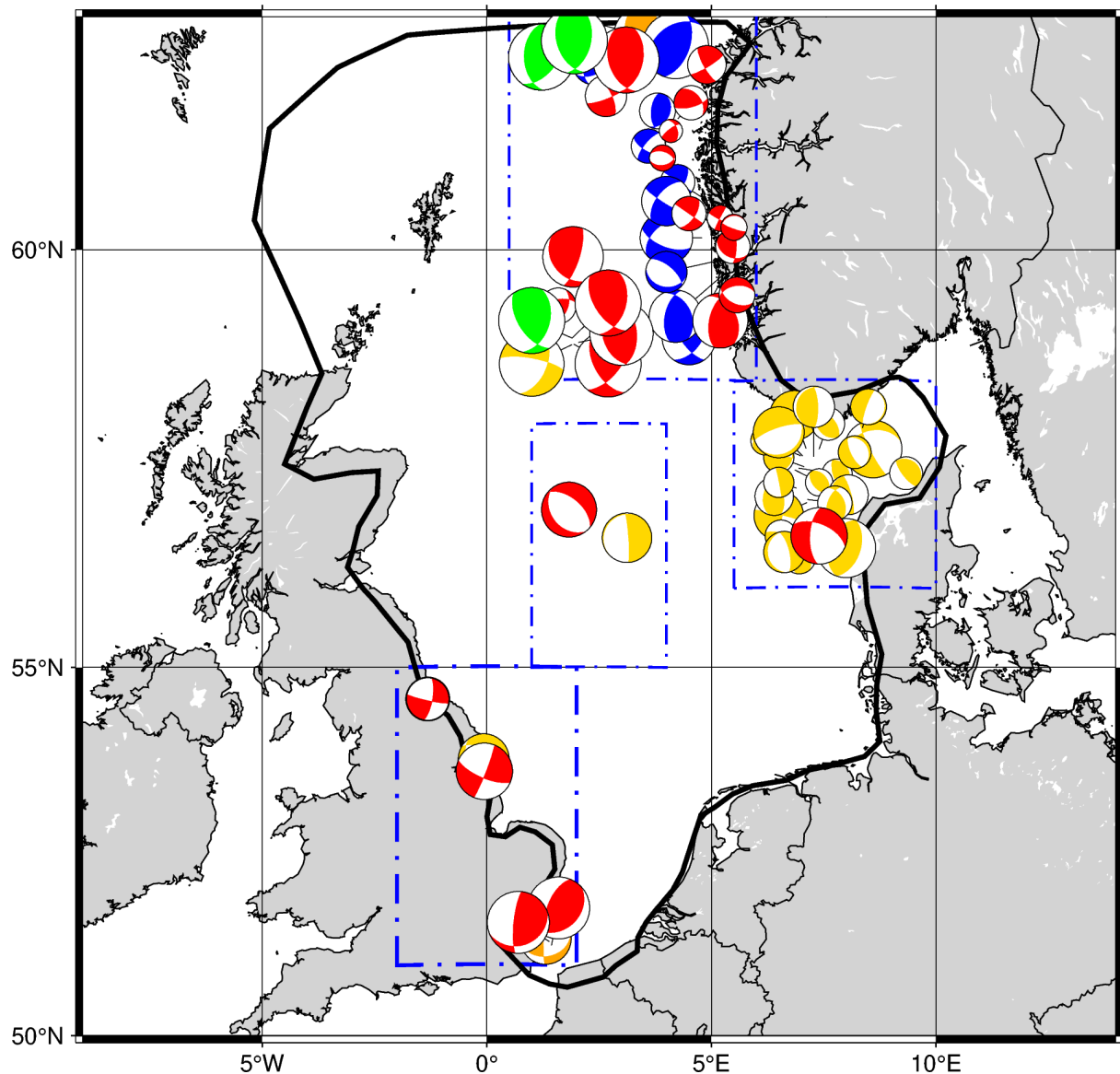


Figure 4.11: Initial focal mechanism catalogue for the North Sea area. Colours mark reporting institutions: green – GCMT, red – ISC, yellow – GEUS, blue – NNSN, orange – GEOFON. Blue rectangles denote regions presented in more detail in the following figures. Mechanism sorted chronologically (more recent overlaying previous events) and hierarchically.

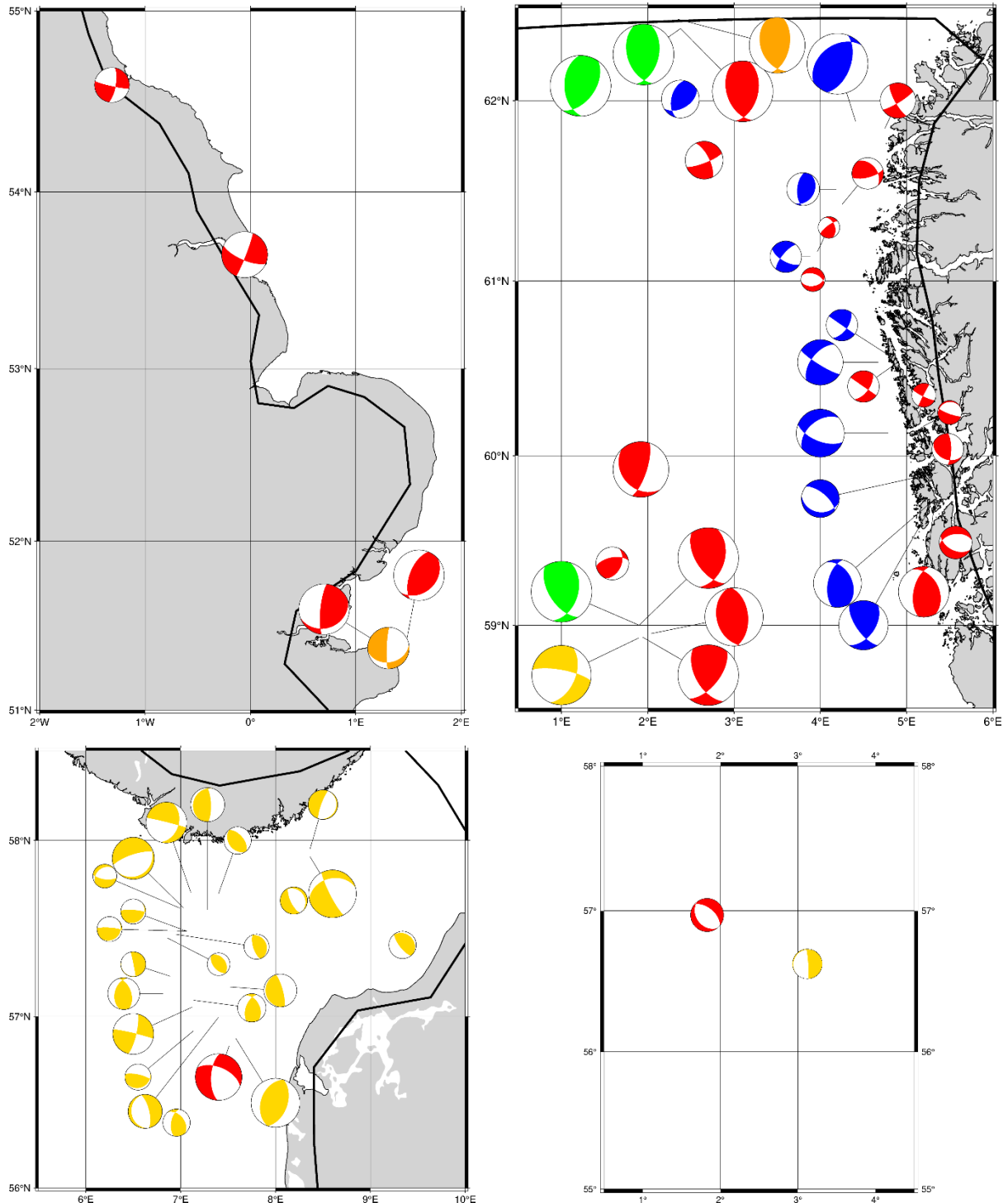


Figure 4.12: Zoom onto UK south coast (top left), Norwegian west coast (top right), Skagerrak (bottom left) and central North Sea (bottom right). See Figure 4.11 for explanation of colours.

A comparison between the focal mechanism catalogue and the event bulletin (Figure 4.12) highlights events for which it may be especially valuable to estimate moment tensors. This concerns for example regions exhibiting seismicity of which so far, no mechanisms seem to have been analyzed (at least within the catalogues we considered, and larger magnitude events whose source mechanisms seem not to have been resolved so far. The most interesting subregions are displayed magnified in Figures A.1 to A.4 in the Appendix.

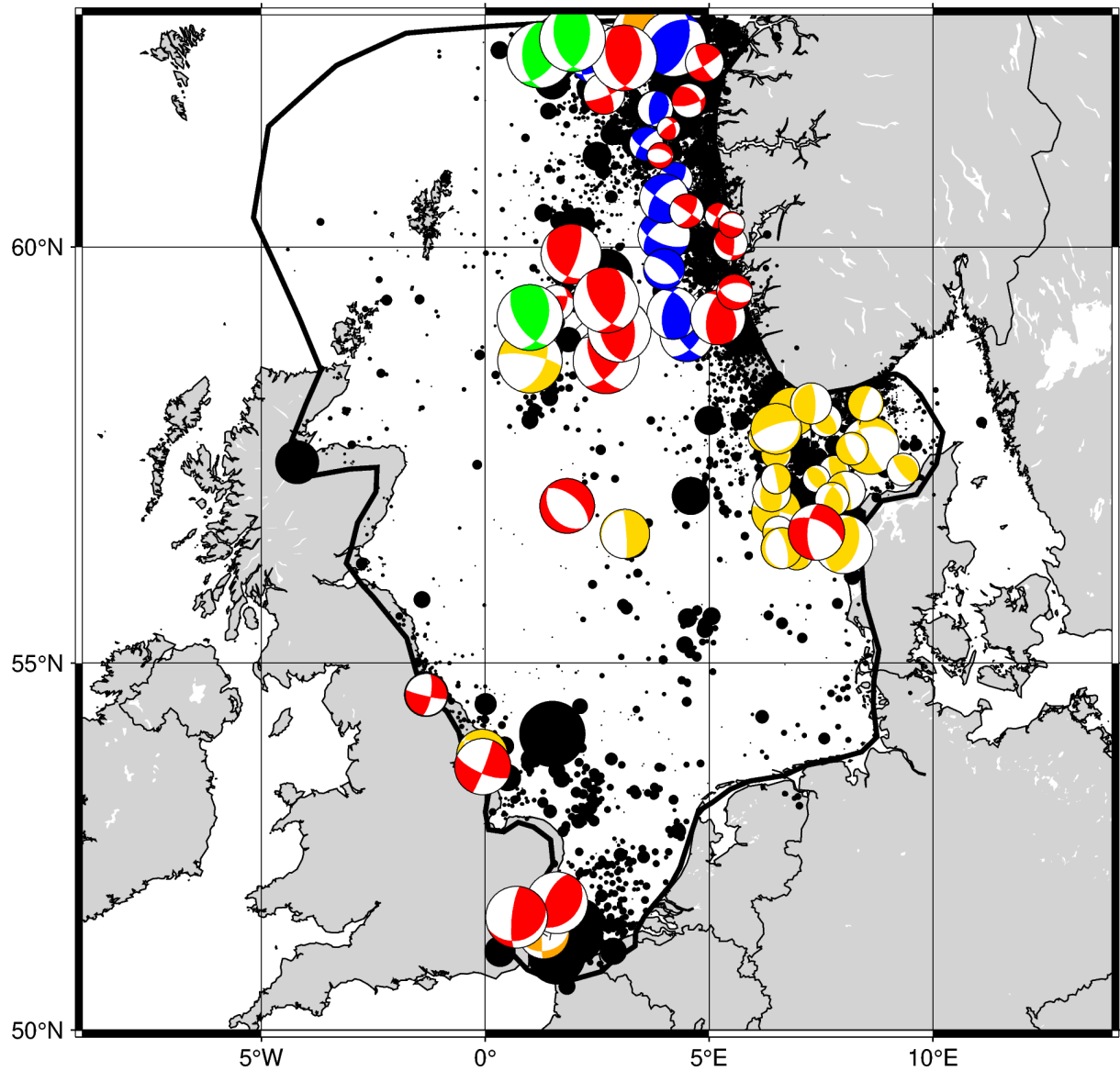


Figure 4.12: Comparison between focal mechanism catalogue (see Figure 4.11 for explanation of colours) and primary entries in event bulletin displayed as black dots sized according to magnitude. Mechanism sorted chronologically and hierarchically.

## 5. Velocity model

One-dimensional velocity models were obtained from various national seismological surveys associated with the countries bordering the North Sea. In addition, we retrieved two laterally varying velocity models frequently used in the scientific literature. These velocity models and some of their characteristics are presented and compared in Section 5.1. In particular, we synthesize an average 1D velocity model. In Section 5.2, we compare these models to models encountered in the scientific literature.

### 5.1 Preparation of a 1D average model for the North Sea

We prepared a 1-D average velocity model for the North Sea in order to analyse tectonic events with respect to their source properties or to enable event relocation. Since the data we will employ for these tasks at first will have been recorded by onshore stations at larger distances, the model needs to consider the deeper crustal layers as well, but with less detail due to the relatively long wavelengths, since shorter wavelengths will be damped during the propagation. In case seismological data becomes available recorded at shorter distances to events (e.g., provided by one of the industry partners), for example within the regions of interest specified in the project, especially the shallow crustal layers of the velocity model need to be updated with more details.

Table 5.1: List of models investigated to prepare a 1D model for the North Sea.

MODEL NAME	DESCRIPTION	COUNTRY WERE MODEL IS USED	MAXIMUM DEPTH (KM)	VP	VS
BGR_GER	Germany-wide	Germany	30	✓	✓
BGR_HAN	North German Basin	Germany	8	✓	✓
BGS CENTRAL NS	Central North Sea	UK	31	✓	✓
BGS DOVER NS	Dover Straits	UK	35	✓	✓
BGS SOUTH NS	South North Sea	UK	34	✓	✓
NORTH NETH	North Netherlands	Netherlands	24.4	✓	✗
SOUTH NETH	South Netherlands	Netherlands	30	✓	✗
GEUS	Denmark-wide	Denmark	80	✓	✓
UIB	NNSN network (Havskov & Bungum, 1987)	Norway	50	✓	✓
NORSAR	NORSAR bulletin (Mykkeltveit & Ringdahl, 1981)	Norway	95	✓	✓
IASP91	IASP91	World	6371	✓	✓
CRUST	CRUST1.0	World	Variable	✓	✓

As a first step, we analysed ten models specifically used for seismic monitoring in the countries bordering the North Sea (Figure 5.1). In addition, the IASP91<sup>1</sup> (Kennet & Engdahl, 1991) as well as CRUST1.0<sup>2</sup> models (Laske et al., 2013) for the North Sea area were investigated (Table 1). CRUST1.0

<sup>1</sup> downloaded from: <http://ds.iris.edu/spud/earthmodel/9991809>, last accessed 02.02.2022

<sup>2</sup> downloaded from: <http://igppweb.ucsd.edu/~gabi/rem.html>, last accessed 30.03.2022

models were extracted with an intergrid point distance of  $0.5^\circ$ , resulting in 114 models for the North Sea area.

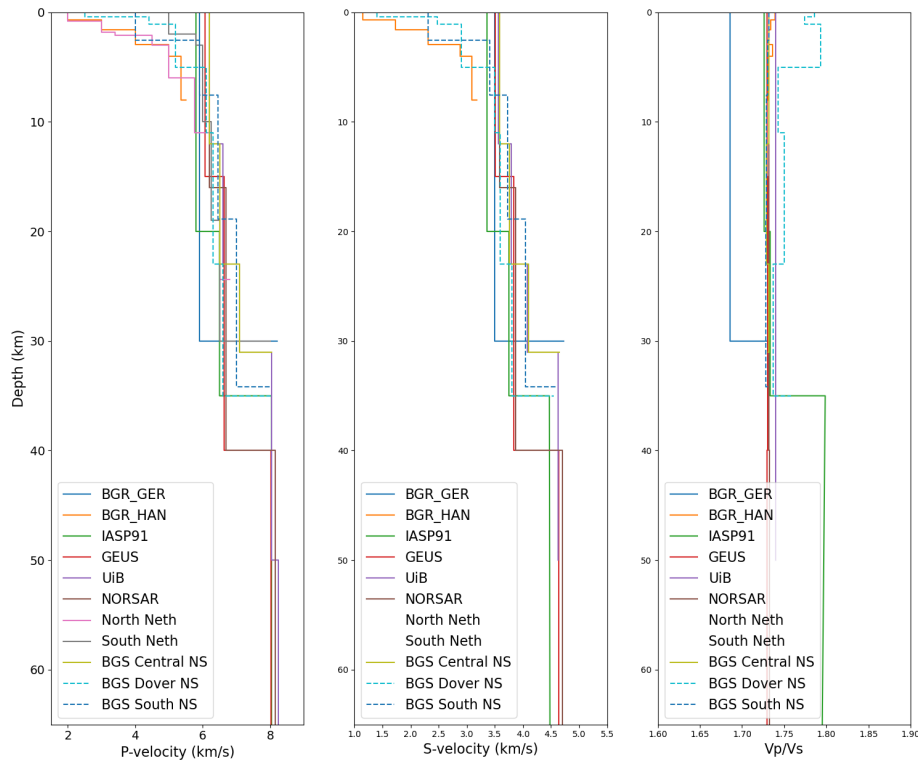


Figure 5.1: Models used for seismic monitoring in the countries bordering the North Sea.

Especially models BGS Central NS, IASP91, BGR\_GER, GEUS and BGS Dover NS possess significantly higher P-wave velocities at the surface. In the following analysis, we disregard models that do not extend in depth to the Moho, since we regard this interface as important for modelling of waveforms for source mechanism. Further, we disregard models without shear wave velocity information. As a result of this initial filtering, the BGR\_HAN, North Neth, South Neth and GEUS models were eliminated, leaving a total of eight models for further analysis.

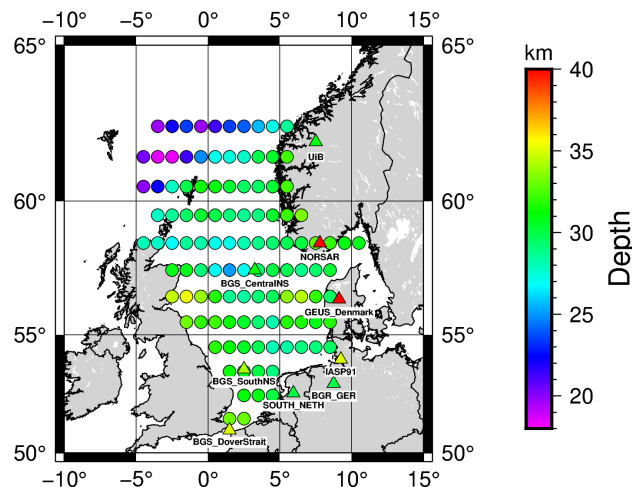


Figure 5.2: Moho depth in the different velocity models. Triangles are arbitrarily located near the area where they are in use for seismic monitoring. Circles correspond to the actual locations of points extracted from the CRUST1.0 model.

Subsequently, the consistency of the depth of the Moho interface among models was analysed (Figure 5.2). Both the NORSAR and GEUS models present a significantly larger Moho depth (~40 km), which probably is more representative of a continental area.

As further criterium, we analysed the properties of the shallower layers comprising the compressional and shear wave velocity of the uppermost layer and the depth of the first interface. In this case, significant differences in detail were observed among the models (Figure 5.3). The CRUST1.0 model displays consistent interface depths and wave propagation velocities within the North Sea area but shows significant variations near coastal regions.

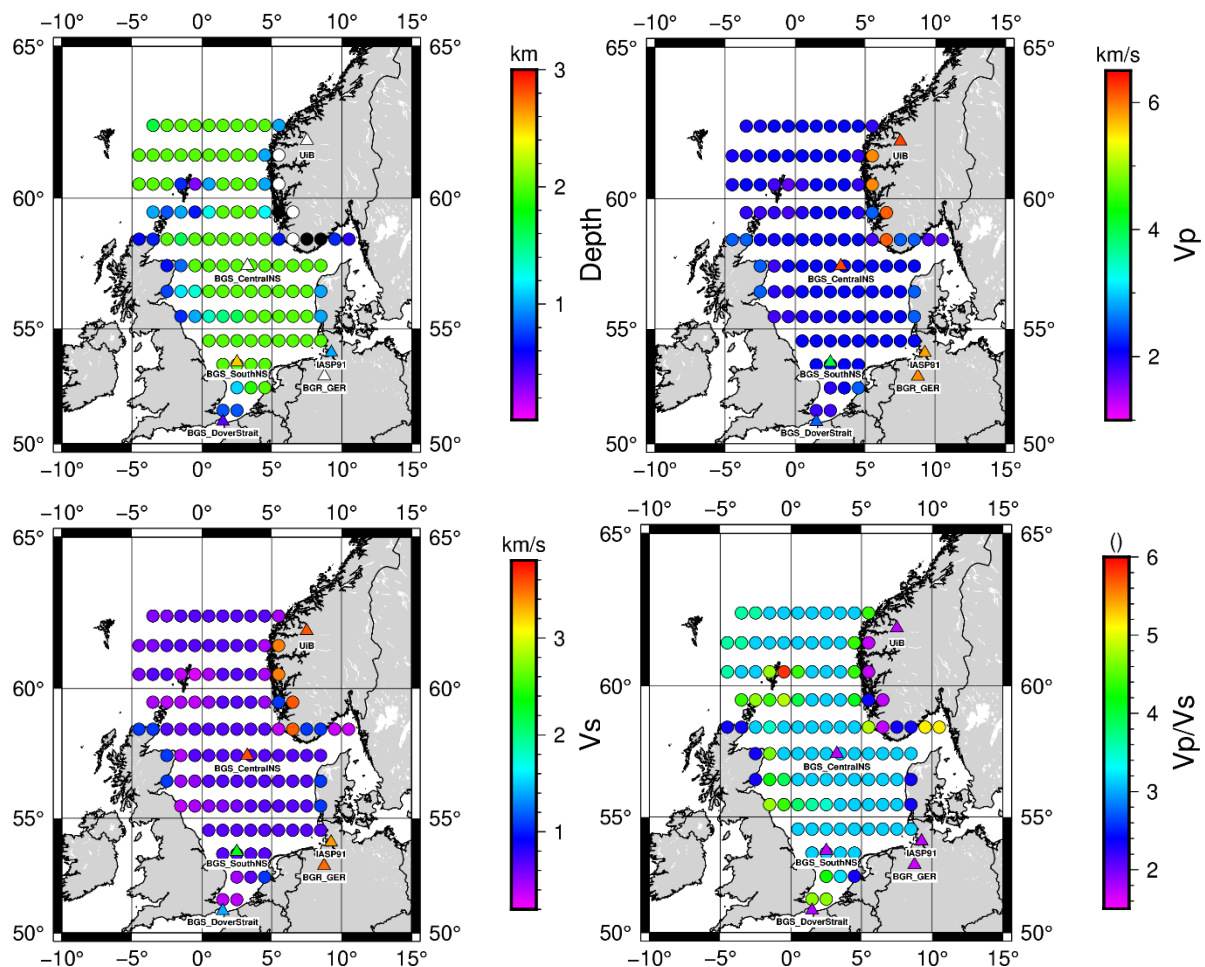


Figure 5.3: Map views showing the depth of the first layer in the different velocity models together with the values of compressional velocity ( $V_p$ ), shear velocity ( $V_s$ ), and compressional to shear velocity ratio ( $V_p/V_s$ ). Symbols explained in Figure 5.2.

In addition, the velocity models employed by the different countries for seismic monitoring displayed significant differences in depth and properties of their shallowest layers compared to the more consistent properties within the North Sea area presented in the CRUST1.0 model (Figure 5.3). Thus, for the purpose of synthesizing an average 1D model for the North Sea, only models from CRUST1.0 within the North Sea area were considered (Figure 5.4, top). To this end, models containing the same number of layers were combined into a single 1D model by applying a median to both the depths of the interfaces and the wave propagation velocities. Figure 5.4 (bottom) displays a comparison of the

compressional velocity profiles between the median 1D model and the CRUST1.0 models used in the median for different values of latitude (see Figure A.5 in the appendix for a comparison of S-wave velocities). The average model is given in the appendix.

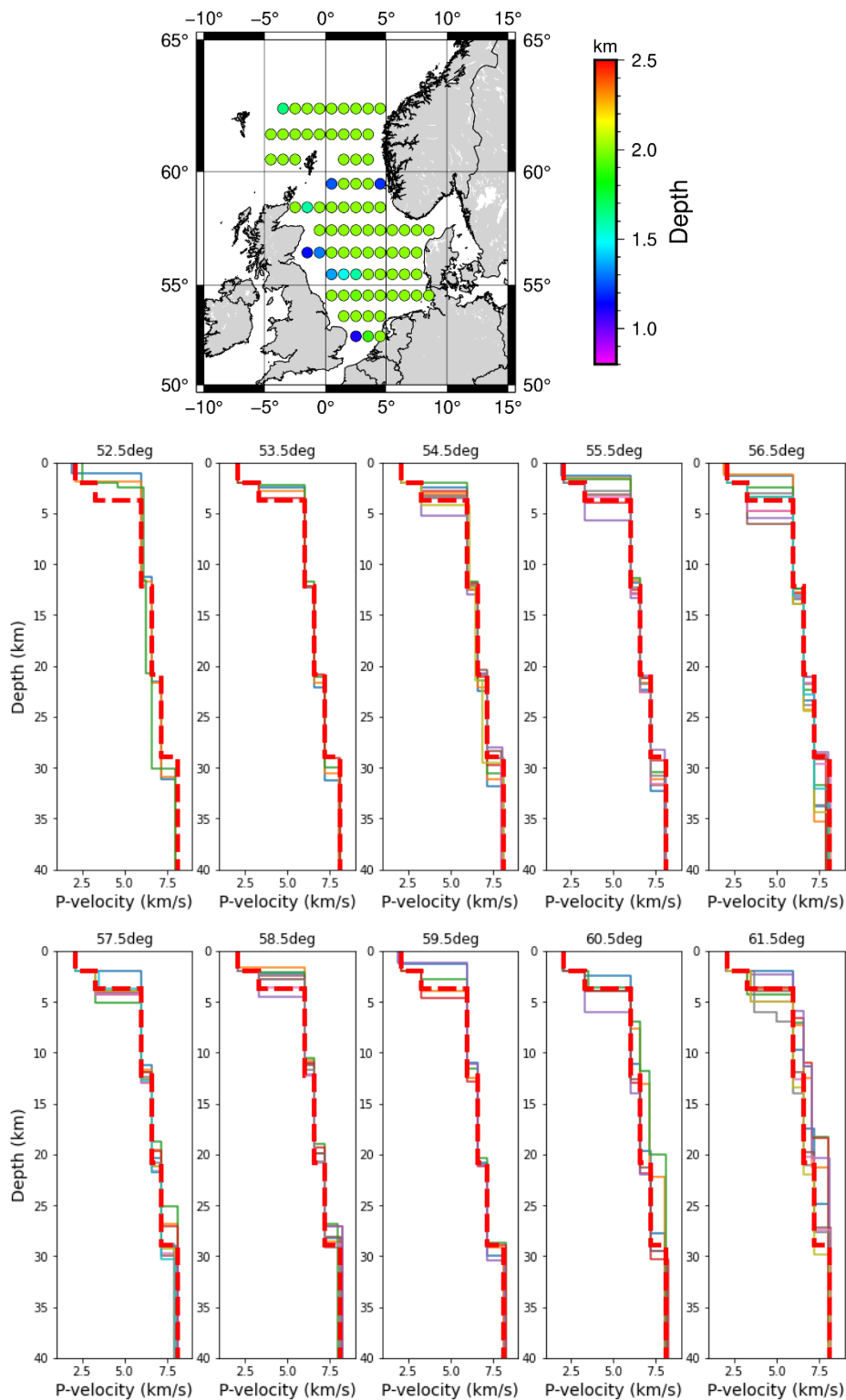


Figure 5.4: Top: map view showing depths to the first interface for the CRUST1.0 model that were used to synthesize an average 1D model for the North Sea. Bottom: comparison between the P-wave velocities in the median 1D model (red dashed line) and the CRUST1.0 models used in the median at different latitudes (indicated at the top of the subfigures).

Finally, Figure 5.5 presents the median 1D model together with the CRUST1.0 models that were not considered for the median near Norway, the UK and Denmark. As additional reference, the models used for seismic monitoring within those countries are shown. Figure 5.6 displays a comparison of the average model with the IASP91 models as well as models used in the Netherlands and Germany for seismic monitoring.

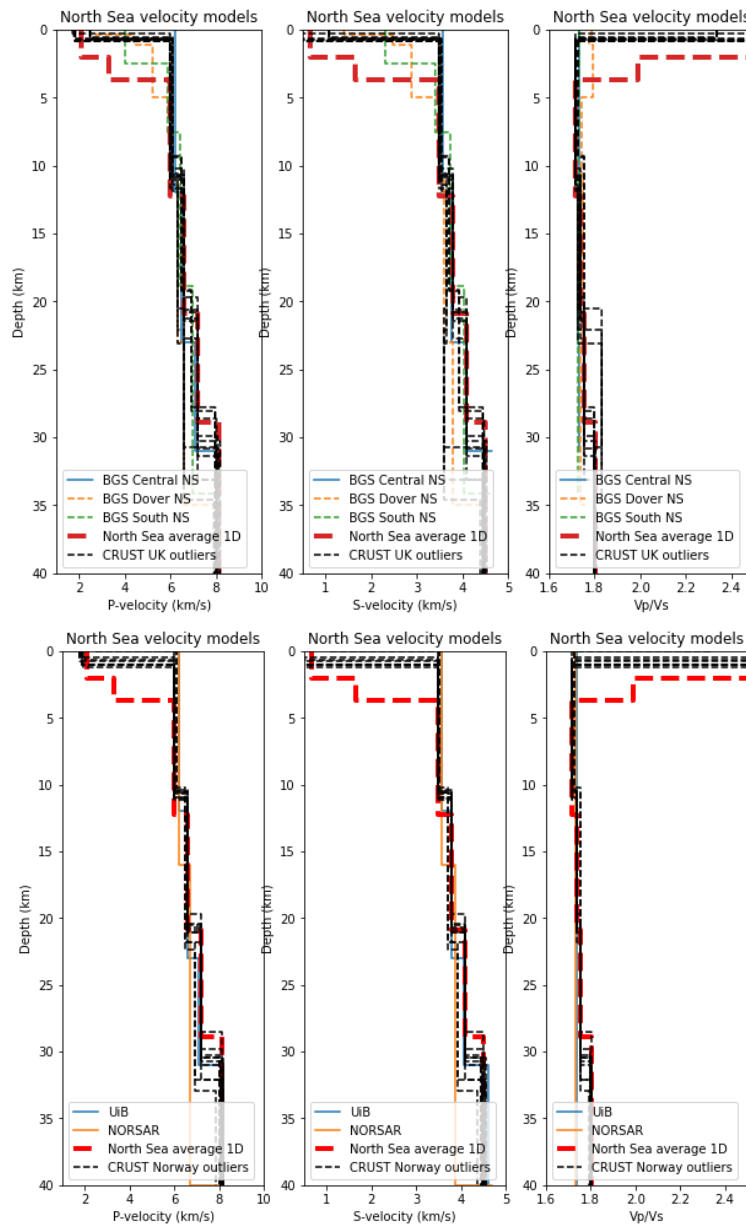


Figure 5.5: Comparison of velocity profiles between the median 1D model (red dashed lines) and the models discarded for the median near the UK (top), Norway (middle) and Denmark (bottom; next page).

SHARP Storage – Project no 327342

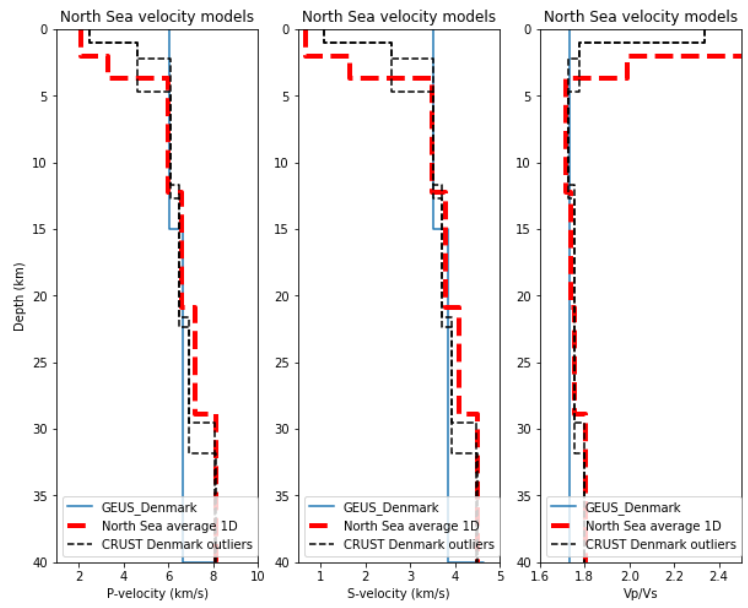


Figure 5.5 (continued)

### SHARP Storage – Project no 327342

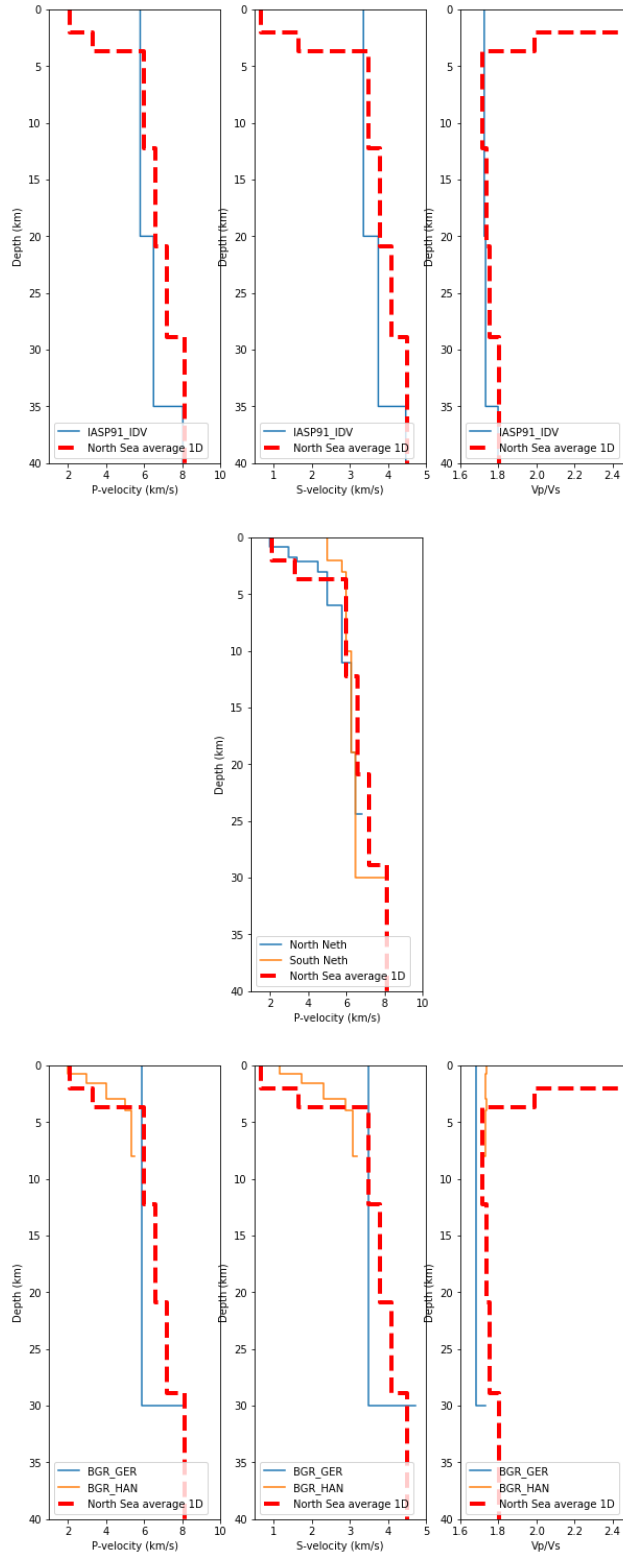


Figure 5.6: Comparison of velocity profiles between the median 1D model (red dashed lines) and the IASP91 model (top) as well as models used for seismic monitoring in the Netherlands (middle) and Germany (bottom). Only a P-wave model was available for the Netherlands.

## 5.2 Comparison with previous models from literature

The present North Sea is a site of a triple plate collision zone during the Caledonian orogeny at the end of the Ordovician and Early Silurian (Abramovitz et al., 1998). This collision involved two continents (Laurentia and Baltica) as well as the Gondwana-derived micro-continent of East Avalonia. Prior to this collision, a narrow ocean, the Tornquist Sea, separated Baltica and East Avalonia (Cocks and Fortey, 1982). The suture zone between both is represented by the Caledonian Deformation Front (CDF) (Abramovitz et al., 1998). Later papers describe two subduction zones involved in the process, the Thor Suture and the Dowsing-South Hewett Fault Zone (Crowder et al., 2021). From the analysis of the active seismic MONA LISA profile 1 in the southeastern North Sea west of Denmark, Abramovitz et al., (1998, 1999) describe the Baltica crust north of the CDF by a high-velocity, three-layered shield type crust and the East Avalonian crust by a low-velocity two-layered crust (Abramovitz et al., 1999). The total crustal thickness decreases southwards from ~35 km towards ~30 km in the central part of the MONA LISA 1 profile and further to ~25 km in its south. The layer disappearing between both parts is the lower crust. The transitional suture zone type crust in the central part of the North Sea is part of the S-SW dipping Caledonian Deformation front. Whereas the P-wave velocity is higher above the Moho for the Baltica crust, as is typical for old shield type crusts, its sub-moho velocities are lower (7.8-7.9 km/s) than for the East Avalonian crust (8.1-8.3 km/s; (Abramovitz et al., 1999). Findings were similar for the MONA LISA 2 profile located 50-100 km further to the west (Abramovitz et al., 2000), however, the upper mantle velocity structure was significantly different in both profiles, showing a velocity increasing laterally from north to south beneath the ML1 profile.

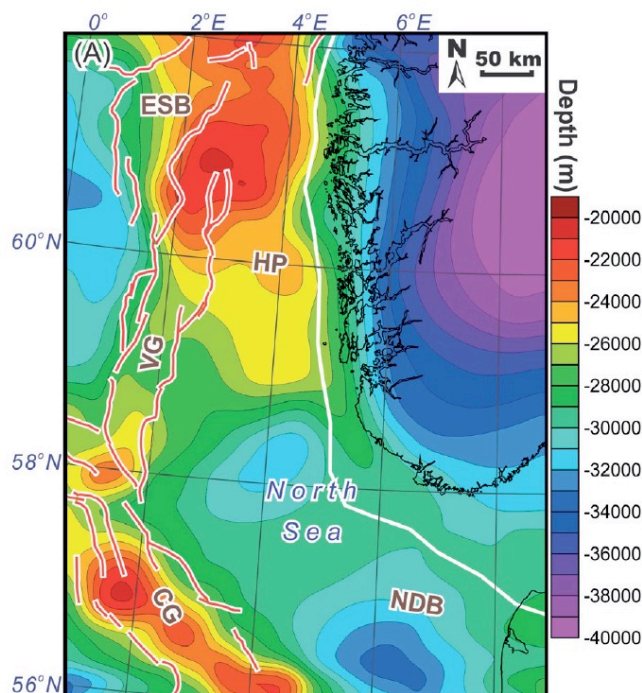


Figure 5.7: Depth to Moho from gravimetric and magnetic modelling (ESB: East Shetland Basin, HP: Horda Platform, VG: Viking Graben, NDB: Norwegian Danish Basin, CG: Central Graben). Figure taken from Maystrenko et al. (2017).

Earlier work in compiling and digitizing seismic data was performed with the aim of presenting Moho maps (Zervos, 1987; Holliger and Klemperer, 1989; Chadwick & Pharaoh, 1998; Grad et al., 2009) or

building a 3D velocity model for the North Sea area (Clegg & England, 2003; Kelly et al., 2007). For the uppermost layers, the model of Kelly et al. (2007) showed significant lateral velocity variations caused by the sedimentary basins up to depths of 10 km. At greater depths, the lower crust on the northwest side of the North Sea Central Graben exhibited higher velocities than in the southeast. Maystrenko et al. (2017) prepared a lithosphere-scale 3D structural model of the northern North Sea and adjacent Norwegian mainland by integrating all available structural data in combination with 3D density and magnetic modelling. Based on the magnetic properties, the structural model was differentiated into smaller crustal blocks. A prominent middle-upper crustal magmatic intrusion was found within the northern part of the Norwegian-Danish Basin. A low-density lithospheric mantle was modelled beneath NW Norway and adjacent offshore areas, most probably reflecting an upper-mantle low-velocity zone. The obtained Moho topography mirrors the major tectonic units of the study area (Figure 5.7). Specifically, it is prominently uplifted to 20 km beneath the Central and Viking Grabens (Maystrenko et al., 2017).

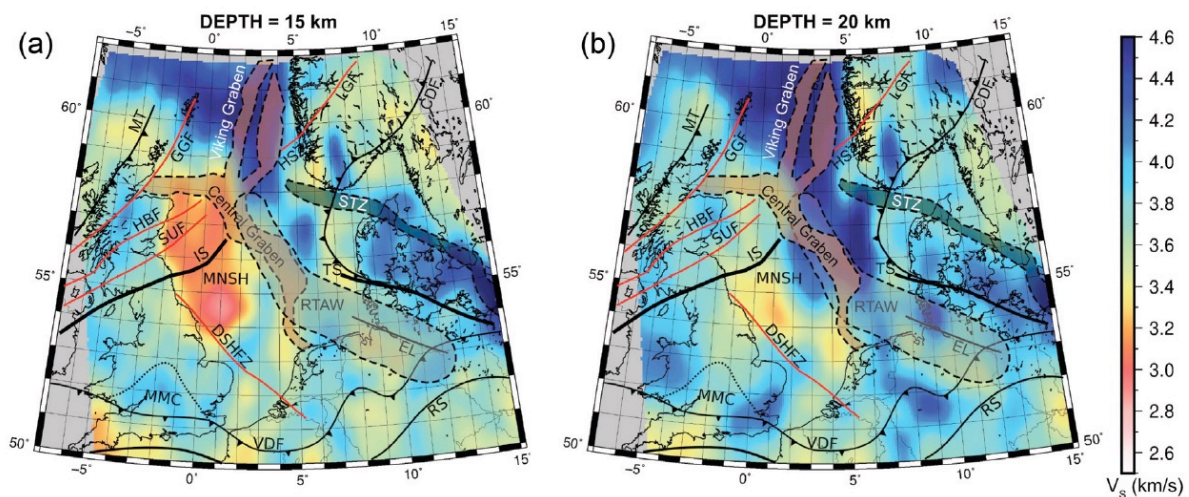


Figure 5.8: Major tectonic features in the North Sea area overlain onto depth slices through final S-wave velocity model at (a) 15 km and (b) 20 km depth: MT (Moine Thrust), GGF (Great Glen Fault), HBF (Highland Boundary Fault), SUF (Southern Uplands Fault), IS (Iapetus Suture), MNSH (Mid-North Sea High), DSHFZ (Dowsing South Hewett Fault Zone), MMC (Midland Microcraton), VDF (Variscan Deformation Front), LSB (Lower Saxony Basin), RS (Rheic Suture), EL (Elbe Lineament), TS (Thor Suture), STZ (Sorgenfrei-Tornquist Zone), HSZ (Hardangerfjord Shear Zone), LGF (Lærdal-Gjende Faults), CDF (Caledonian Deformation Front), RTAW (Remnant Thor Accretionary Wedge). Figure taken from Crowder et al. (2021).

As recent as in 2021, Crowder et al. note that the deep crustal structure beneath the North Sea is still poorly understood, since it is constrained by only a few deep seismic reflection and refraction profiles in contrast to its sedimentary basins hosting hydrocarbon source rocks and reservoirs, which are therefore well explored and understood (Fichler et al., 2011). Thus, Crowder et al. (2021) aimed to provide a 3-D shear wave velocity model to constrain crustal properties to ~30 km depth beneath the North Sea and surrounding landmasses from ambient noise tomography (Figure 5.8). Such studies in the North Sea area are notoriously difficult due to high noise levels in the North Sea, dominant noise sources within the study area, the high attenuation in the crust and the complexity of the recovered signal (Crowder et al., 2021). In this model, the major sedimentary basins appear as low shear-wave velocity zones (< 2.9 km/s) matching published sediment thickness maps. Relatively high velocities (~3.5 km/s) in the Mid North Sea High region are typical of granites and greenschist. The crustal

thickness varies from 13-18 km beneath the Central Graben to 25-30 km elsewhere. The known failed rift system of the North Sea, which was active from the Triassic to the Jurassic and ceased during the Cretaceous, seems to be related to the locations of the Laurentia-Avalonia-Baltica palaeoplate boundaries (see Figure 5.9 for the main tectonic features).

The thinning of the Moho in the Central North Sea is also recognisable in the CRUST1.0 models, albeit with lower resolution, but can of course not be captured in an averaged 1-D velocity model. The averaged model, however, reproduces the low P- and S-wave velocities of the huge sedimentary basins better than most of the models employed by countries bordering the North Sea for seismic monitoring (Figure 5.5, Figure 5.6). Depending on which part of the waveform is inverted for moment tensor inversion, the well-known North Sea Lg blockage for wave paths across graben structures associated with sedimentary basin formation and crustal thinning potentially needs to be taken into account (Gregersen, 1984; Maupin, 1989; Mendi et al., 1997), since this effect will not be captured by the current 1D velocity model as well.

According to Crowder et al. (2021), the Horda platform, a key study area of this project, is located along with the Viking Graben in a region of thinned crust. Gabrielsen et al. (1990) state that the Permo-Triassic rifting is especially distinct on the Horda platform and in the Shetland basin, involving major fault systems as e.g the Øygarden fault complex; especially the N-S striking faults became reactivated during the Jurassic Cretaceous development of the Viking Graben. Maystrenko et al. (2017) interpret a low-density upper-crustal block beneath the Horda platform as possible presence of metasedimentary or fractured granitic rocks as opposed to the relatively dense granitic rocks potentially forming the middle-crustal layer beneath its southern part. A high-velocity lower-crustal body beneath the platform was explained by Christiansson et al. (2000) as deep crustal root of partially eclogitized rocks formed during the Caledonian orogeny.

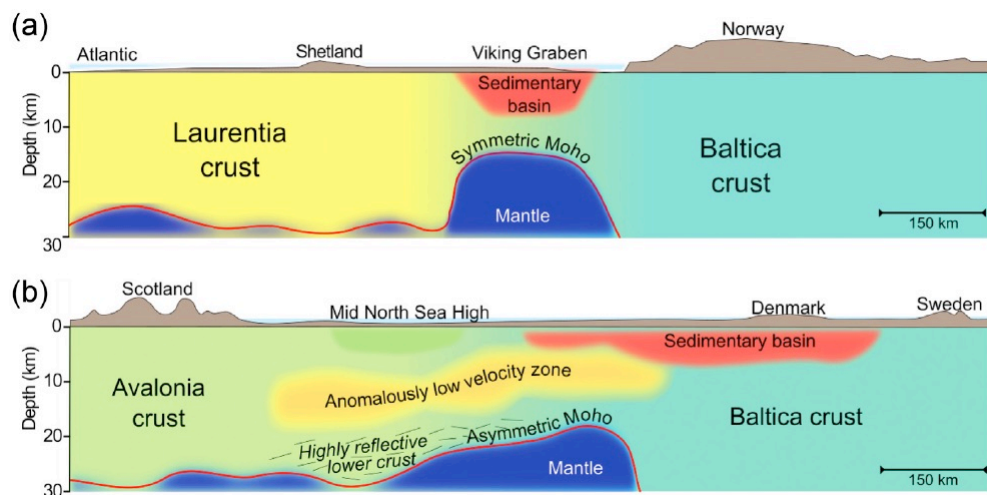


Figure 5.9: Sketch of key features in the North Sea. (a) symmetric thinning of the crust in the northern North Sea between the crust of Laurentia and Baltica origin; (b) asymmetric thinning of the crust of Avalonia and Baltica origin. Figure taken from Crowder et al. (2021).

## 6. References

- Abramovitz, T., Thybo, H. & MONA LISA Working Group (1998). Seismic structure across the Caledonian Deformation Front along MONA LISA profile 1 in the southeastern North Sea. *Tectonophysics*, **288**, 153-176.
- Abramovitz, T., Landes, M., Thybo, H., Brian Jacob, A.W. & Prodehl, C. (1999). Crustal velocity structure across the Tornquist and Iapetus Suture Zones – a comparison based on MONA LISA and VARNET data. *Tectonophysics*, **314**, 69-82.
- Abramovitz, T. & Thybo, H. (2000). Seismic images of Caledonian, lithosphere-scale collision structures in the southeastern North Sea along Mona Lisa Profile 2. *Tectonophysics*, **317**(1-2), 27-54.
- Aki, K. (1965). Maximum likelihood estimate of  $b$  in the formula  $\log N = a - bM$  and its confidence. *Bulletin of Earthquake Research Institute of the University of Tokyo*, **43**, 237–239.
- Cao, A., & Gao, S. S. (2002). Temporal variation of seismic  $b$ -values beneath northeastern Japan island arc. *Geophysical Research Letters*, **29**(9), 48-1-48–3. <https://doi.org/10.1029/2001gl013775>
- Chadwick, R. A. & Pharaoh, T. C. (1998). The seismic reflection Moho beneath the United Kingdom and adjacent areas. *Tectonophysics*, **299**(4), 255-279.
- Christiansson, P., Faleide, J. I. & Berge, A. M. (2000). Crustal structure in the northern North Sea: an integrated geophysical study. *Geol.Soc., London, Special Publ.*, **167**(1), 15-40.
- Clegg, B. & England, R. (2003). Velocity structure of the UK continental shelf from a compilation of wide-angle and refraction data. *Geol.Mag.*, **140**(4), 453-467.
- Cocks, I.R.M. & Fortey, R.A. (1982). Faunal evidence for oceanic separations in the Palaeozoic of Britain. *J. Geol. Soc., London*, **139**, 465-478.
- Crowder, E., Rawlinson, N., Cornwell, D.G., Sammarco, C., Galetti, E. & Curtis, A. (2021). New insights into North Sea deep crustal structure and extension from transdimensional ambient noise tomography. *Geophys. J. Int.*, **224**, 1197-1210.
- Deichmann, N. (2017). Theoretical Basis for the Observed Break in  $M_L / M_W$  Scaling between Small and Large Earthquakes. *Bulletin of the Seismological Society of America*, **107**(2). <https://doi.org/10.1785/0120160318>
- Dziewonski, A. M., Chou, T.-A. & Woodhouse, J. H. (1981). Determination of earthquake source parameters from waveform data for studies of global and regional seismicity. *J. Geophys. Res.*, **86**, 2825-2852.
- Ekström, G., Nettles, M. & Dziewonski, A. M. (2012). The global CMT project 2004-2010: Centroid-moment tensors for 13,017 earthquakes, *Phys. Earth Planet. Inter.*, **200-201**, 1-9.
- Fichler, C., Odinsen, T., Rueslåtten, H., Olesen, O., Vindstad, J. E., & Wienecke, S. (2011). Crustal inhomogeneities in the Northern North Sea from potential field modeling: inherited structure and serpentinites?. *Tectonophysics*, **510**(1-2), 172-185.

- Gabrielsen, R.H., Færseth, R.B., Steel, R.J., Idil, S. & Kløvjan, O.S. (1990). Architectural styles of basin fill in the northern Viking Graben, in *Tectonic Evolution of the North Sea Rifts*, edited by D. J. Blundell and A. D. Gibbs, pp. 158–179, Clarendon Press, Oxford, Calif.
- Grad, M., Tiira, T. & ESC Working Group. (2009). The Moho depth map of the European Plate. *Geophys. J. Int.*, **176**(1), 279-292.
- Gregersen, S. (1984). Lg-wave propagation and crustal structure differences near Denmark and the North Sea. *Geophys. J. Int.*, **79**(1), 217-234.
- Havskov, J. & Bungum, H. (1987): Source parameters for earthquakes in the northern North Sea. *Norsk Geol. Tids.*, **67**, 51-58.
- Heidbach, O., M. Rajabi, K. Reiter, M.O. Ziegler & the WSM Team (2016). World Stress Map Database Release 2016. GFZ Data Services, [doi:10.5880/WSM.2016.001](https://doi.org/10.5880/WSM.2016.001).
- Holliger, K. & Klemperer, S.L. (1989). A comparison of the Moho interpreted from gravity data and from deep seismic reflection data in the northern North Sea. *Geophys. J. Int.*, **97**(2), 247-258.
- International Seismological Center (ISC), IASPEI Seismic Format (ISF), <http://www.isc.ac.uk/standards/isf> (last access: 23 September 2022). International Seismological Centre (2022). On-line Bulletin. <https://doi.org/10.31905/D808B830>.
- Jónasson, K., Bessason, B., Helgadóttir, Á., Einarsson, P., Guðmundsson, G. B., Brandsdóttir, B., Vogfjörð, K. S., & Jónsdóttir, K. (2197). A harmonised instrumental earthquake catalogue for Iceland and the northern Mid-Atlantic Ridge. *Hazards Earth Syst. Sci*, **21**. <https://doi.org/10.5194/nhess-21-2197-2021>
- Jones, A., Michael, A., Simpson, B., Jacob, S., & Oppenheimer, D. (2000). Rapid Distribution of Earthquake Information for Everybody. *Seismological Research Letters*, **71**(3), 355–358. <https://doi.org/10.1785/GSSRL.71.3.355>
- Kelly, A., England, R.W. & Maguire, P. K. (2007). A crustal seismic velocity model for the UK, Ireland and surrounding seas. *Geophys. J. Int.*, **171**(3), 1172-1184.
- Kennett, B.L.N. & Engdahl, E.R. (1991). Travel times for global earthquake location and phase identification. *Geophys. J. Int.*, **105**, 429-466, doi: 10.1111/j.1365-246X.1991.tb06724.x.
- Laske, G., Masters, G., Ma, Z. & Pasyanos, M. (2013). Update on CRUST1.0 - A 1-degree global model of Earth's crust. *Geophys. Res. Abstracts*, **15**, Abstract EGU2013-2658 & <https://igppweb.ucsd.edu/~gabi/crust1.html>.
- Lentas, K. (2018). Towards routine determination of focal mechanisms obtained from first motion P-wave arrivals. *Geophys. J. Int.*, **212**(3), 1665–1686.
- Lentas, K., Di Giacomo, D., Harris, J. & Storchak, D. A. (2019). The ISC Bulletin as a comprehensive source of earthquake source mechanisms. *Earth Syst. Sci. Data*, **11**, 565-578.
- Leydecker, G. (2011). Erdbebenkatalog für Deutschland mit Randgebieten für die Jahre 800 bis 2008. *Geol. Jahrbuch*, E 59, pp. 1-198; Hannover, Germany
- Marzocchi, W., & Sandri, L. (2003). A review and new insights on the estimation of the b-value and its uncertainty. *Annals of Geophysics*, **46**(6), 1271–1282. <https://doi.org/10.4401/ag-3472>

Maupin, V. (1989). Numerical modelling of Lg wave propagation across the North Sea Central Graben. *Geophys. J. Int.*, **99**(2), 273-283.

Maystrenko, Y.P., Olesen, O., Ebbing, J. & Nasuti, A. (2017). Deep structure of the northern North sea and southwestern Norway based on 3D density and magnetic modelling. *Norwegian J. Geol.*, **97**, 169-210.

Mendi, C. D., Ruud, B. O., & Husebye, E. S. (1997). The North Sea Lg-blockage puzzle. *Geophys. J. Int.*, **130**(3), 669-680.

Mykkeltveit, S. & Ringdal, F. (1981). Phase identification and event location at regional distance using small-aperture array data. In: *Identification of seismic sources - earthquake or underground explosion* (eds. Husebye, E.S. & Mykkeltveit, S.), 467-481.

NORSAR (1971a). NORSAR seismic bulletins, doi: 10.21348/b.0001.

NORSAR (1971b). NORSAR Station Network [Data set], doi: 10.21348/d.no.0001.

Quinteros, J., Strollo, A., Evans, P. L., Hanka, W., Heinloo, A., Hemmleb, S., Hillmann, L., Jäckel, K.-H., Kind, R., Saul, J., Zieke, T. & Tilmann, F. (2021). The GEOFON Program in 2020. *Seismol. Res. Lett.*, **92**(3), 1610–1622.

Roberts, N. S., Bell, A. F., & Main, I. G. (2015). Are volcanic seismic b-values high, and if so when? *Journal of Volcanology and Geothermal Research*, **308**, 127–141. <https://doi.org/10.1016/j.jvolgeores.2015.10.021>

Ruigrok, E., Dost, B., 2019. Seismic monitoring and site-characterization with near-surface vertical arrays, in: *Near Surface Geoscience Conference and Exhibition*. pp. 1–5.

Tinti, S., & Mulargia, F. (1987). Confidence intervals of b values for grouped magnitudes. *Bulletin of the Seismological Society of America*, **77**(6), 2125–2134.

<http://www.bssaonline.org/content/77/6/2125.abstract>

Tjåland, N. & Ottemöller, L. (2018). Evaluation of seismicity in the northern North Sea. *NNSN Tech. Rep.*, **29**, University of Bergen.

Tjåland, N. (2020). Determination of fault plane solutions using P-wave polarities. *NNSN Tech. Rep.*, University of Bergen.

University of Bergen. (1982). *University of Bergen Seismic Network* [Data set]. International Federation of Digital Seismograph Network, doi: 10.7914/SN/NS

Zarifi, Z., Hansteen, F., Schopper, F., 2021. Seismic Moment Tensor Inversion of an Induced Microseismic Event, Offshore Norway: An Insight into the Possible Cause of Wellbore Liner Failure during a Drilling Operation. *Seismological Research Letters* **92**, 3460–3470.

Zervos, F. (1987). A compilation and regional interpretation of the northern North Sea gravity map. *Geol. Soc., London, Special Publ.*, **28**(1), 477-493.

## A. Appendix

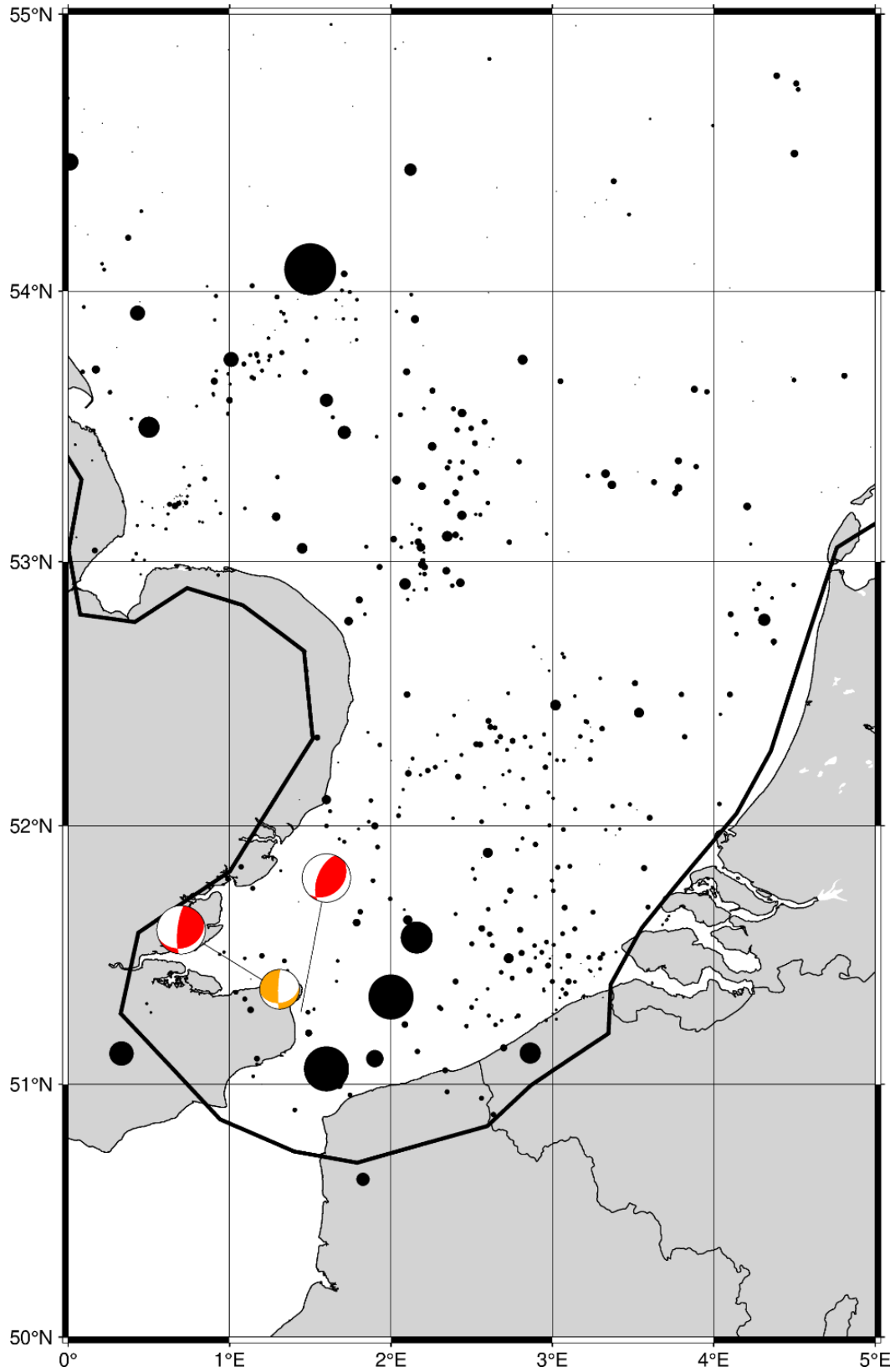


Figure A.1: Comparison between focal mechanism catalogue (see Figure 4.11 for explanation of colours) and primary entries in event bulletin displayed as black dots sized according to magnitude; zoom on rectangular subregion from 0° to 5°E and 50°N to 55°N.

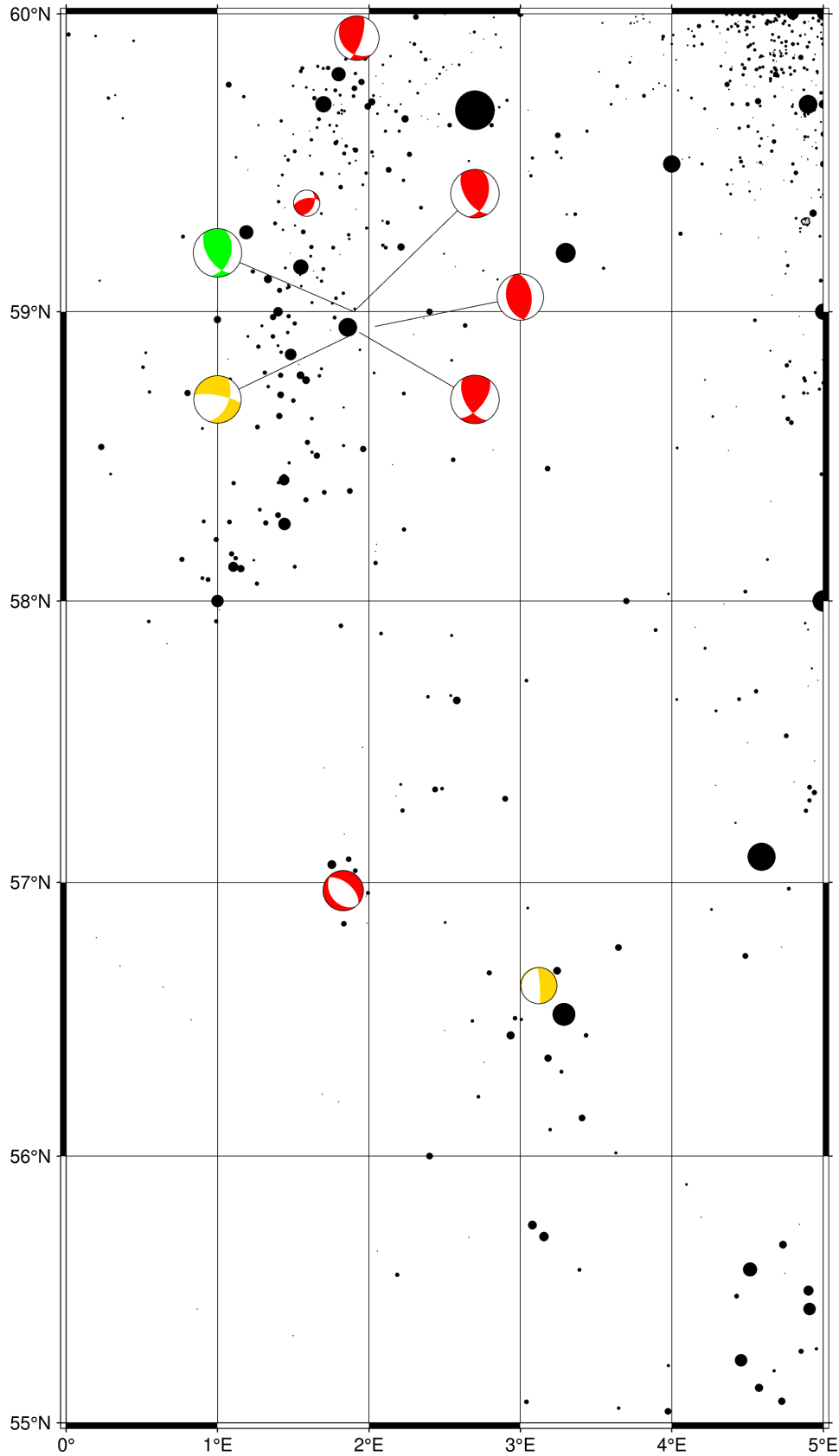


Figure A.2: Comparison between focal mechanism catalogue (see Figure 4.11 for explanation of colours) and primary entries in event bulletin displayed as black dots sized according to magnitude; zoom on rectangular subregion from 0° to 5°E and 55°N to 60°N.

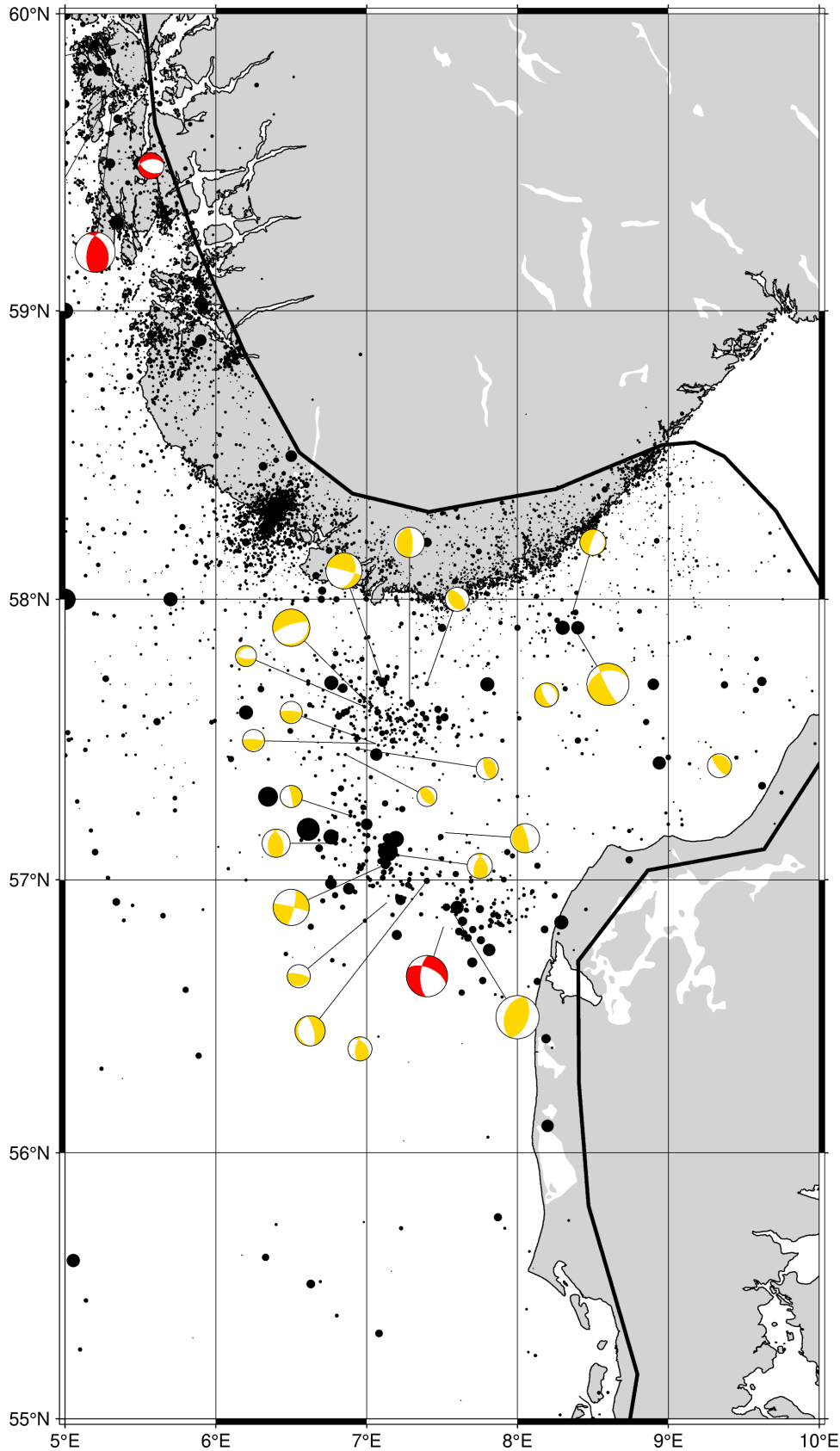


Figure. A.3: Comparison between focal mechanism catalogue (see Figure 4.11 for explanation of colours) and primary entries in event bulletin displayed as black dots sized according to magnitude; zoom on rectangular subregion from 5°E to 10°E and 55°N to 60°N.

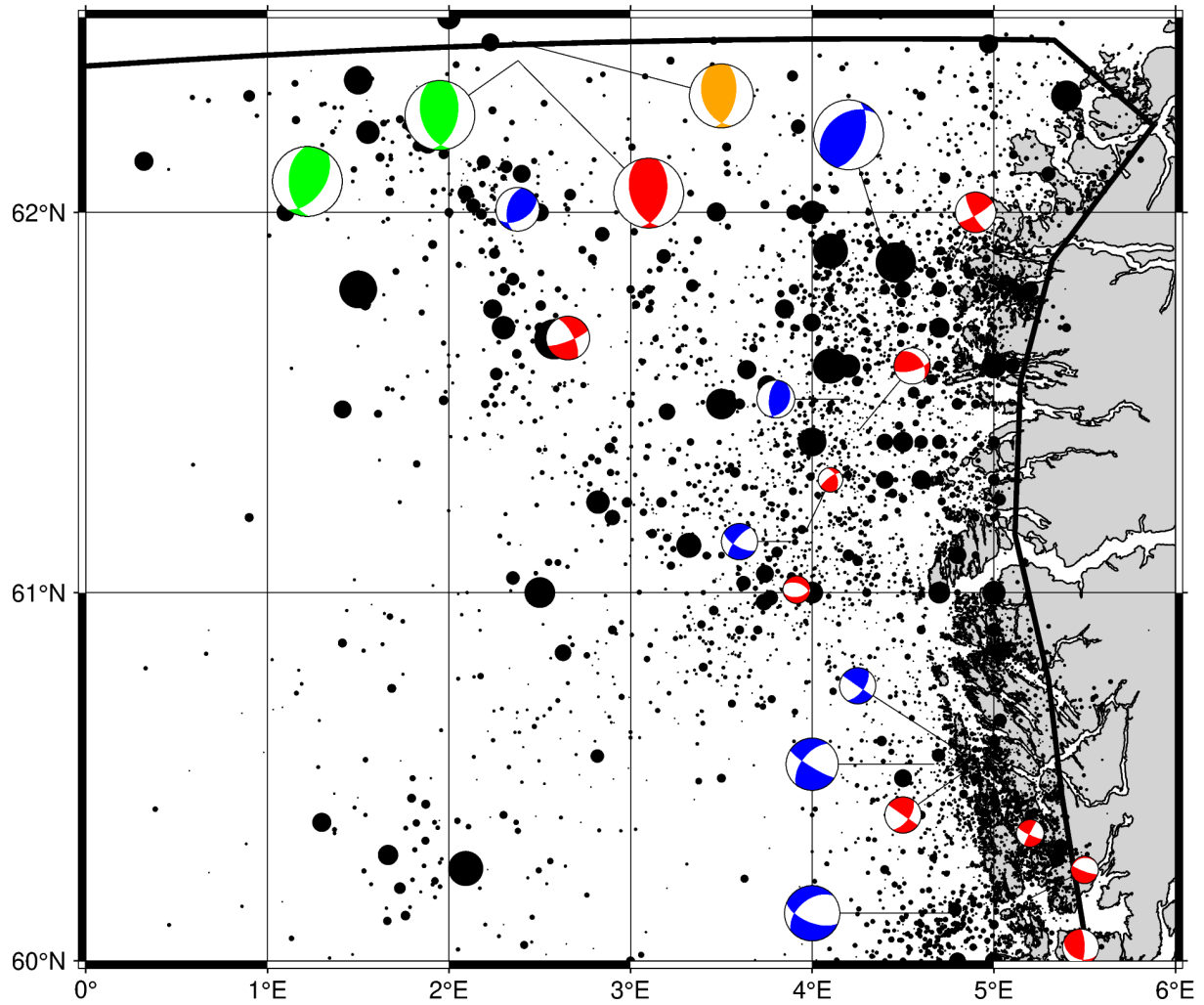


Figure A.4: Comparison between focal mechanism catalogue (see Figure 4.11 for explanation of colours) and primary entries in event bulletin displayed as black dots sized according to magnitude; zoom on rectangular subregion from 0°E to 6°E and 60°N to 62.5°N.

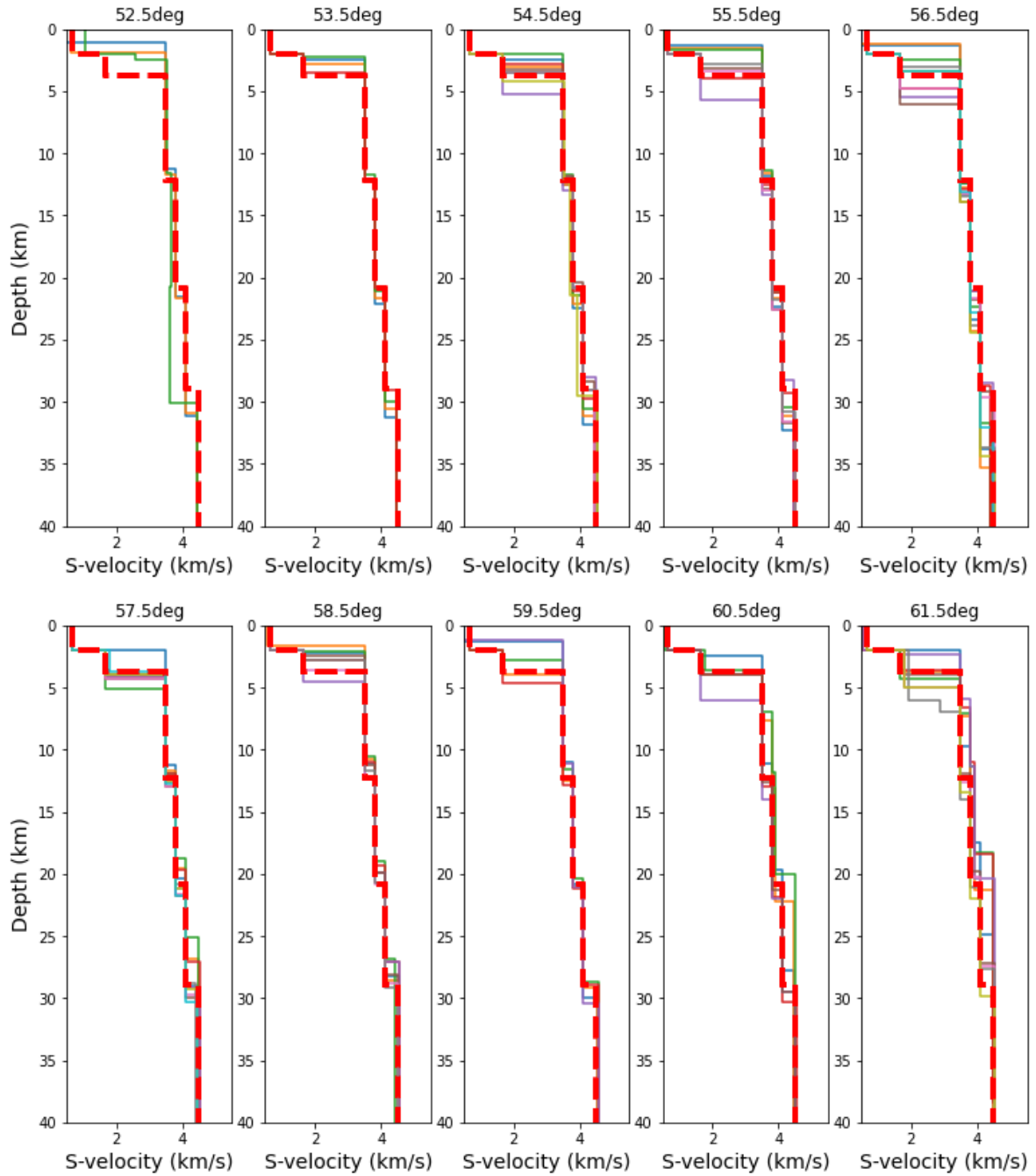


Figure A.5: Comparison between the S-wave velocities in the median 1D model (red dashed line) and the CRUST1.0 models used in the median at different latitudes (indicated at the top of the subfigures).